Satellite remote sensing of Arctic fires

– a literature and data review

Kerstin Stebel

TITLE	PROJECT LEADER
	Kerstin Stebel
Satellite remote sensing of Arctic fires – a literature and data review	**NILU PROJECT NO.**
	S-121071

AUTHOR(S)	QUALITY CONTROLLER
Kerstin Stebel	Arve Kylling

REPORT PREPARED FOR	CONTRACT REF.
Norsk Romsenter, Postboks 113 Skøyen, 0212 Oslo Att.: Anja Sundal	74CO2107

ABSTRACT

The main aim of this report is to prepare for the proposed SGA #17 of the Caroline Herschel Framework Partnership Agreement on Copernicus User Uptake Work Programme 2020 named "Arctic peat- and forest-fire information system".

First, we summarize the scientific background of wildfires in the Arctic and the Northern boreal zone and describe observations of long-range transport of forest fire pollution. This is followed by an overview of satellite data and resources available for fire monitoring in these regions. This covers the fire ECVs, as well as smoke plume tracers. Furthermore, we list CAMS and CEMS resources, i.e., GWIS, EFFIS (including the latest country report for Norway), and GFAS, as well as other fire emission inventories. Knowledge gaps and limitations of satellite remote sensing, future missions, Norwegian user uptake and user groups are described.

NORWEGIAN TITLE

Fjernmåling av arktiske branner – en litteratur- og datagjennomgang

KEYWORDS

remote sensing	Arctic	fire

ABSTRACT (in Norwegian)

Hovedmålet med rapporten er å forberede det foreslåtte SGA #17 i Caroline Herschel Framework Partnership Agreement on Copernicus User Uptake Work Program 2020 kalt "Arktisk torv- og skogbranninformasjonssystem".

Først oppsummerer vi den vitenskapelige kunnskapsbasen om skogbranner i Arktis og den nordlige boreale sonen og beskriver observasjoner av forurensning fra skogbranner i Arktis. Deretter følger en oversikt over satellittdata og ressurser tilgjengelig for brannovervåking i disse regionene. Dette inkluderer brann-ECV-ene, samt langtransporterte forurensninger. Videre presenterer vi CAMS- og CEMS-ressurser, dvs. GWIS, EFFIS (inkludert rapporten for Norge), og GFAS, samt andre brannutslippsinventarer. Kunnskapshull og begrensninger ved satellittfjernmåling, fremtidige satellittinstrumenter, og norsk brukeropptak og brukergrupper er beskrevet.

PUBLICATION TYPE: Digital document (pdf)	COVER PICTURE: Source: NILU

Citation: Stebel, K., (2023). Satellite remote sensing of Arctic fires – a literature and data review (NILU report 29/2022). Kjeller: NILU.

Contents

Summary

The main aim of the "Satellite remote sensing of Arctic fires – a literature and data review" report is to prepare for the proposed Specific Grant Agreements (SGA) #17 of the Caroline Herschel Framework Partnership Agreement on Copernicus User Uptake Work Programme 2020 named "Arctic peat- and forest-fire information system".

First, we summarize the scientific background of wildfires in the Arctic and the Northern boreal zone and describe observations of long-range transport of forest fire pollution. This is followed by an overview of satellite data and resources available for fire monitoring in these regions. This covers the fire Essential Climate Variables, i.e., burned area, active fire maps, and fire radiative power, as well as smoke plume tracers. Furthermore, we present relevant Copernicus Atmospheric Monitoring Services and Copernicus Emergency Monitoring Services resources, i.e., the Global Wildfire Information System, the European Forest Fire Information System – including the country report for Norway, and the Global Fire Assimilation System, as well as other fire emission inventories. Finally, knowledge gaps and limitations of satellite remote sensing, future missions, Norwegian user uptake and user groups are described.

Satellite remote sensing of Arctic fires
– a literature and data review

Acronyms

AAI	Aerosol Absorbing Index
AC SAF	Satellite Application Facility on Atmospheric Composition Monitoring
AOD	Aerosol optical thickness
AMAP	Arctic Monitoring and Assessment Program
ASTER	Advanced Spaceborne Thermal Emission and Reflection radiometer
ATLID	Atmospheric Lidar
AVHRR	Advanced Very High-Resolution Radiometer
BIRA-ISAB	Royal Belgian Institute for Space Aeronomy
BIRD	Bi-Spectral Infrared Detection
BIROS	Bi-spectral InfraRed Optical System
BBR	Broad-Band Radiometer
BRIS	Brann, Redning, Innrapportering, Statistikk
CALIOP	Cloud-Aerosol Lidar with Orthogonal Polarization
CALIPSO	Cloud-Aerosol Lidar and Infrared Pathfinder Satellite Observations
CAMS	Copernicus Atmosphere Monitoring Service
CAVM	Circumpolar Arctic Vegetation Map
CCI	Climate Change Initiative
C3S	Copernicus Climate Change Service
CDS	Copernicus climate data store
CEOS	Committee on Earth Observing Satellites
CEMS	Copernicus Emergency Management Service
CICERO	Center for International Climate Research
CNES	Centre national d'études spatiales (National Center for Space Studies)
CO	carbon monoxide
CO2	carbon dioxide
CPR	Cloud Profiling Radar
DLR	Deutsche Gesellschaft für Luft und Raumfahrt (German-Aerospace-Center
DSB	Directorate for Civil Protection
EarthCARE	Earth Clouds, Aerosols and Radiation Explorer
ECV	Essential Climate Variable
ECMWF	European Centre for Medium-Range Weather Forecasts
EFFIS	European Forest Fire Information System
EO	Earth observation
EOSDIS	Earth Observing System Data and Information System
EPS-SG	EUMETSAT Polar System Second Generation
EUMETSAT	European Organisation for the Exploitation of Meteorological Satellites
EMS	Emergency Management Service
ESA	European Space Agency
FEER	Fire Energetics and Emissions Research
FINN	Fire inventory from National Center for Atmospheric Research
FIRMS	Fire Information for Resource Management System
FLEX	FLuorescence EXplorer
FLORIS	Fluorescence Imaging Spectrometer
FMI	Finnish Meteorological Institute
FRIC	Fire Research and Innovation Centre
FRP	Fire Radiative Power

FWI	Fire Weather Index
GCOS	Global Climate Observing System
GFAS	Global Fire Assimilation System
GOME-2	Global Ozone Monitoring Experiment-2
HVL	Western Norway University of Applied Sciences
IASI	Infrared Atmospheric Sounding Interferometer
IASI-NG	Infrared Atmospheric Sounder Interferometer-Next Generation
IFS	Integrated Forecast System
IPCC	Intergovernmental Panel on Climate Change
IR	infrared
JRC	Joint Research Centre
Landsat	Land Remote-Sensing Satellite
LP DAAC	Land Processes Distributed Active Archive Center
LSA-SAF	Satellite Application Facility on Land Surface Analysis
LTDR	Land Long Term Data Record
LWIR	long-wave infrared
NASA	National Aeronautics and Space Administration
NCAR	National Center for Atmospheric Research
NIBIO	Norwegian Institute of Bioeconomy Research
NICFI	Norway's International Climate & Forests Initiative
NILU	Norwegian Institute for Air Research
NIR	near infrared
NOAA	National Oceanic and Atmospheric Administration
NRT	near real time
NTC	non-time critical
NTNU	Norwegian University of Science and Technology
NWP	numerical weather prediction
MET	Norwegian Meteorological Institute
MIR	Middle infrared
MODIS	Moderate Resolution Imaging Spectroradiometer
MSI	Multi-Spectral Imager
MWIR	mid-wave infrared
OLCI	Ocean and Land Colour Instrument
OLI	Operational Land Imager
OMI	Ozone Monitoring Instrument
OMPS	Ozone Mapping and Profiler Suite
pyroCbs	pyro cumulonimbus
QFED	Quick Fire Emissions Dataset
radar	radio detection and ranging
SACS	Support to Aviation Control Service
SAMPO	Satellite Measurements from Polar Orbit
SEVIRI	Spinning Enhanced Visible and InfraRed Imager
SINTEF	Foundation for Scientific and Industrial Research at the Norwegian Institute of Technology
SLSTR	Sea and Land Surface Temperature Radiometer
Suomi NPP	Suomi National Polar orbiting Partnership
SWIR	short wave infrared
TET	Technology Experiment Carrier
TIR	thermal infrared
TOMS	Total Ozone Mapping Spectrometer
TROPOMI	TROPOspheric Monitoring Instrument
UTLS	upper troposphere / lower stratosphere
UVAI	UV Aerosol Index
VIIRS	Visible Infrared Imaging Radiometer Suite
VNF	VIIRS Nightfire
WBKZ	Waldbrannkennziffer
3MI	Multi-view Multi-channel Multi-polarization Imager

1 Introduction

In the following we shortly describe the scientific background of wildfires (hereafter just "fires") in the Arctic and the Northern boreal zone and describe observations of long-range transport of forest fire pollution.

1.1 Fires - in the Arctic and the Northern boreal forest

Fires are characterized by large spatial and temporal variations (diurnally, seasonally, and inter-annually). They can consume vegetation, emit trace gases and aerosols, reduce air quality, affect human health, and impact the global carbon storage. Fires can lead to low visibility and pose a risk for aviation. Timely and accurate quantification of fire activity and impacts on global, regional, and national level are needed for informed policy- and decision making.

The impact of climate change on fires is complex, but recent models suggest that a warming climate can lead to increased wildfires, which can reinforce Arctic warming. To quote the recent Intergovernmental Panel on Climate Change (IPCC[1]) summary report for policy makers: "*Human influence has likely increased the chance of compound extreme events since the 1950s. This includes increases in the frequency of concurrent heatwaves and droughts on the global scale (high confidence), fire weather in some regions of all inhabited continents (medium confidence), and compound flooding in some locations (medium confidence)*" and "*It is virtually certain that the Arctic will continue to warm more than global surface temperature, with high confidence above two times the rate of global warming*" (IPCC, 2021).

Climate change and human activity increase fire risk in many regions, including the Arctic, and high latitude boreal ecosystems (e.g., McCarty et al. (2021) and references therein). This is linked to increased natural lightning strikes (e.g., Veraverbeke et al. 2017), permafrost thawing (Osterkamp 2005; Gibson et al., 2018, Holloway et al., 2020, Swanson et al. 2021), vegetation shift, and more human-caused ignitions (e.g., Sizov et al. 2021). With global temperatures increasing, wildfires are becoming more frequent and more intense (Abatzoglou et al., 2019). Record-breaking wildfire seasons have been seen across the world in recent years, from Australia to the Arctic, to North and South America. Even the Arctic, previously unaffected, now faces rising wildfire risk (United Nations Environment Programme, 2022). Large fires were seen in Canada (2016), Greenland (2017, 2019), Fennoscandia (2018), Alaska (2019), and Russia (2018, 2019, 2020). Fires in Greenland are a new phenomenon, and a local source of black carbon deposition on the Greenland ice sheet (Evangeliou et al., 2019) with albedo change, that may contribute to accelerated melting of the Greenland ice sheet (Keegan et al., 2014). Favourable fire weather (persistent hot, dry, and windy) occurred in 2019 and 2020 in Siberia. A heatwave with persistent warm anomalies across Siberia lasted from January to June 2020. Temperatures as high as 38°C were recorded on 20th June 2020 at Verkhoyansk (67.55°N, 133.38°E) (Ciavarella et al. 2020). The unprecedented fires burned tens of millions of hectares, releasing 0.244 Gt CO_2 into the atmosphere (Witze, 2020). In the Sakha Republic, the burned area was greater than 2.9 times the 20-year mean in both 2019 and 2020 (York et al., 2020).

Megafires, i.e., extraordinarily large fires, are not only important due to their devastating effects, but they also represent a major contribution to the upper tropospheric and, occasionally, also to the stratospheric, aerosol load worldwide. Intense heat from the fires and atmospheric water vapor initiates pyrocumolonimbus (pyroCbs) storms with smoke injected into the stratosphere (Fromm et al., 2010). In this category falls the 2009 "Black Saturday" bushfires in Australia (e.g., Glatthor et al., 2013), the wildfires in British Columbia in August 2017 (Torres et al., 2020), and the 2019/2020 eastern Australian bush fires (e.g., Kloss et al., 2021, Boer et al., 2020). Ohneiser et al. (2020) identified an

---

[1] https://www.ipcc.ch/

upper troposphere / lower stratosphere (UTLS) smoke layer over the North Pole region in the winter months of 2019–2020 as emissions from 2019 **Siberian wildfires**, which were brought upward, likely by a self-lifting effects (in the absence of pyroCb convection).

Northern **peatlands** hold ~80% of the global peatland carbon (C) and nitrogen (N) stocks (Hugelius et al. 2020). At present, peatlands cool the climate, but anthropogenic warming can lead to thawing of permafrost peatlands, making them vulnerable to fires, and can eventually shift them into a net source of warming (Hugelius et al. 2020). Smouldering peat can emit large amounts of smoke. See Hu et al. (2018) for a review of the emissions from smouldering peat fires and their contribution to regional haze episodes. Peatland fires can burn surface vegetation as well in portions of the underground peat layer. They can smoulder for months, years, or even decades (Hu et al., 2018), burn laterally and vertically deep into the organic soil, and can release smoke at a different location. They can smoulder through the non-fire season, appear extinguished, but flare up in the subsequent fire season, thus being referred to as **holdover, overwintered, or "zombie" fires** (see e.g., McCarty et al. 2020, Scholten et al., 2021, Xu et al., 2022).

Compared to the millions of hectares of forest burned e.g., in the north-central Russian Arctic in 2020, the number of fires and total burned area in **Norway** are low. Nevertheless, Norway and its northern-most outpost in Svalbard, where the Zeppelin Mountain monitoring station (78.9°N, 11.9°E., 474 a.s.l.) is located, are regularly affected by long range transport of pollution from fires in other regions. Furthermore, to quote the recent European Forest Fire Information System (EFFIS) country report: "*In Norway, more extreme events are expected as results of climate change, with more precipitation, but also increasing temperatures and droughts. This can imply increase growth in grass, shrubs, and trees, overgrowing of cultural landscapes, a longer fire season and larger fires as a result of more fuel*" (Botnen, 2021).

1.2 Long-range transport of biomass burning emissions seen in the Arctic

Fires emit aerosol and gases into the atmosphere. The transport of fire pollution is determined by weather patterns. The Arctic is regularly affected by smoke from forest fires from Canada, Greenland, Eastern Europe, and Northern Eurasia/Siberia.

Intensive pollution episodes are frequently observed in Svalbard, e.g., at the Zeppelin Mountain observatory, in the villages of Ny-Ålesund, Hornsund, or Barentsburg. Their effect on air quality can be clearly seen in *Figure 1*. Observations of aerosol optical thickness (AOD) show that between 2002 and 2018, these episodes were rare and short in duration (1-3 days) (Kabanov et al., 2020). However, in 2019 high AOD was not limited to few days, but persisted over weeks (Myhre et al., 2020). The link to the 2019 Siberian Forest fires is under evaluation (Hansen, G., personal communication, 04/2022).

Selected events which were observed in the Arctic and reported in the scientific literature are listed below:

- Boreal region biomass burning aerosols in central Alaska and seasonal AOD variation at Barrow, Alaska – overview (Eck et al., 2009).

- Pan-Arctic enhancements of light absorbing aerosol due to North American boreal forest fires in summer 2004 – includes observations from Ny-Ålesund (Stohl et al., 2006, Stone et al., 2008).

- Agricultural fires in Eastern Europe caused very strong pollution levels in the Arctic during spring 2006 – includes observations from Ny-Ålesund (Eckhardt et al., 2007, Lund Myhre et al., 2007, Stohl et al., 2007; Treffeisen et al., 2007).

Figure 1: Adapted from Stohl et al., (2007) Fig. 2. View from the Zeppelin station under clear conditions on 26 April (left panel), and during the smoke episode on 2 May 2006 (right panel). Image courtesy of Ann-Christine Engvall.

- Arctic smoke from early season forest fires and Arctic haze from Russia, was observed in March 2008 – includes observations from Ny-Ålesund (Stock et al., 2012)

- Cross-polar transport of smoke plumes from Siberian Forest fires and anthropogenic sources in East Asian during July 2008 (Sodemann et al., 2011).

- Biomass burning aerosols generated in central Alaska affected Ny-Ålesund in the mid of July 2015 – includes observations from Ny-Ålesund (Markowicz et al., 2016, Markowicz et al., 2017, Moroni et al., 2017, Ritter et al., 2018, Moroni et al., 2020)

- Effects of wildfires in northern Eurasia on black carbon in the Arctic 2002-2013 – model, overview (Evangeliou et al., 2016)

- Wildfires in Greenland in July 2017 are a local source of black carbon on the ice sheet (Evangeliou et al., 2019)

- Long range transport of biomass burning episode which took place in Greenland in summer 2017, extreme smoke event in Canada in August 2017 – includes observations from Ny-Ålesund (Zielinski et al., 2020, Ranjbar et al., 2019)

- Distribution of Atmospheric Aerosol Physicochemical Characteristics in the Russian Sector of the Arctic Ocean – overview paper (Sakerin, 2020).

- Transport of mineral dust from Central Asia and biomass burning emissions from forest fires in Ukraine and south Russia in October 2020 – includes observations from Ny-Ålesund (Groot Zwaaftink et al., 2022)

- Wildfire smoke layer from severe fires in Siberia in July and August 2019 observed over the North pole region – includes observations from Ny-Ålesund (Engelmann et al., 2021, Ohneiser et al., 2021), Transport of Siberian fire emissions to North America (Johnson et al., 2021)

2 Remote sensing of fires

Remote sensing is a powerful tool to identify fire disturbance and to map burned area (e.g., Giglio et al., 2006, 2009, 2018, Schroeder et al., 2014, Chuvieco et al., 2019, Pettinari and Chuvieco, 2020; and references therein), for forecasting (e.g., Pickell et al., 2017), post-fire modelling (e.g., Miller et al., 2017), to estimate impacts on and from fire emissions (Rogers et al., 2020), and for quantification of fire disturbance and recovery (e.g., Hislop et al., 2020). Earth observation also plays an essential role in providing the input for fire emission modelling (see Section 3.3, page 24). Here, we mainly concentrate on **post-fire monitoring**, i.e., fire-detection and their effects. Nevertheless, it should be noted, that remote sensing is a valuable tool for **pre-fire assessment** (e.g., Schneider et al., 2008), as determined by climate and hydrology (precipitation, temperature, soil moisture, fuel moisture, humidity, winds), landscape and vegetation (topography and vegetation conditions).

2.1 Fire ECVs (burned area, active fire maps, fire radiative power) and tracer

The Global Climate Observing System (GCOS) implementation plan, published in 2016, describes the proposed implementation of a global observing system for climate (GCOS, 2016[2]). The fire related Essential Climate Variables (ECV's): active fire maps, burned area, and fire radiative power (FRP) were described (see *Table 1* and *Table 2*).

Table 1: Fire ECV's [adapted from Table 16. Sources of Terrestrial Domain ECV – Biosphere (GCOS, 2016, p172)].

Name	Quantities measured	Measurements	Sources of Data
Fire	**burned area** (m^2) **fire radiative power** (FRP, Watts)	Optical, middle infrared and thermal infrared Geostationary and moderate to high-resolution optical systems continuity required. Daily detection of burned area with horizontal resolution of 250 m and accuracy of 15% FRP horizontal resolutions of 1 km to 0.25 km, time resolution of 30 minutes, with accuracy of 25%	GOFC regional networks[3] GFMC[4] ESA CCI[5] GFED[6] Copernicus[7] LPDAAC[8]

Burned area map burn scars, surfaces affected by fire to display significant changes in the vegetation cover and the ground surface. **Active fires** are located by thermal anomalies (hot spots) they produce. **FRP** is the rate of emitted radiative energy by the fire at the time of the observation. As fires are patchy and heterogeneous, GCOS defines several requirements for their measurements: Global burned area measurements require near-daily observation from moderate (30 m) optical sensors to daily from coarse resolution sensors (250 m – 500 m). These may be complemented by radar remote sensing under cloudy conditions. Active fires and FRP require lower spatial resolution (e.g., 1 km) because of sub-pixel (10^{-4} to 10^{-3} of the pixel area) hotspot detection. Higher resolution (e.g., 250 m – 500 m) is beneficial to detect small fires. Sensors typically operate in the mid-wave infrared spectral channel, a wide dynamic range is needed to avoid saturation, and utilize additional channels in the thermal-infrared, visible and near-infrared to avoid false detection. Low earth observations multiple times per day are needed, with one of the observations in the early afternoon (peak of daily fire cycle). Despite their coarser spatial resolution, geostationary observations are very interesting due to their temporal resolution (e.g., the Spinning Enhanced Visible and InfraRed Imager (SEVIRI): max. 15 minute; the European Organisation for the Exploitation of Meteorological Satellites (EUMETSAT) provides Active

---

[2] https://gcos.wmo.int/en/gcos-implementation-plan

[3] https://gofcgold.org/regional-networks

[4] https://gfmc.online/

[5] https://climate.esa.int/en/projects/fire/

[6] https://www.globalfiredata.org/

[7] https://www.copernicus.eu/en

[8] https://lpdaac.usgs.gov/

Fire monitoring product (FIR[9]), the Satellite Application Facility on Land Surface Analysis (LSA-SAF[10]) provides FRP-pixel[11] products). Unfortunately, the geographical coverage of SEVIRI is restricted to Africa and Europe (plus a small part of South America), therefore these data are not suitable for the detection far Northern boreal forest and in the Arctic region.

Table 2: Terrestrial ECV product requirements [equivalent to Table on page 289 (GCOS, 2016)].

Terrestrial ECV product requirements								
ECV	Products	Frequency	Resolution	Required measurement uncertainty	Stability (per decade unless otherwise specified)	Standards/ References	Entity (see Part II, section 2.2)	
							Satellite	In Situ
Fire	Burnt Areas	24 hours	30 m	15% (error of omission and commission), compared to 30-m observations		None	WGClimate	
	Active fire maps	6 hours at all latitudes from polar-orbiting and 1 hour from geostationary	0.25-1 km (polar); 1–3 km (geo)	5% error of commission 10% error of omission Based on per-fire comparisons for fires above target threshold of 5 MW/km² equivalent integrated FRP per pixel (i.e. for a 0.5 km² pixel the target threshold would be 2.5 MW, for a 9 km² pixel it would be 45 MW).			WGClimate	
	Fire radiative power	6 hours at all latitudes from polar-orbiting and 1 hour from geostationary	0.25-1 km (polar); 1–3 km (geo)	10% integrated over pixel. Based on target detection threshold of 5 MW/km² equivalent integrated FRP per pixel (i.e. for a 0.5 km² pixel the target threshold would be 2.5 MW, for a 9 km² pixel it would be 45 MW).and with the same detection accuracy as the Active Fire Maps.			WGClimate	

In the Best Practices document of the Committee on Earth Observation Satellites (CEOS) Working Group on Calibration and Validation - Land Product Validation Subgroup, the validation status of the fire ECVs have been classified (see *Table 3*). While active fire and burned area have reached a higher maturity level, the validation of the various FRP products require more efforts.

GCOS defined several Actions, addressing historic fire data, operational burned area and FRP, fire maps, validation, and fire disturbance model development, which were commented on in the Space Agency Response to GCOS Implementation Plan[12] (CEOS, 2018). They state the fire ECVs are approaching target requirements with respect to spatial resolution (250 m), for temporal resolution the utilization of merged products from multiple sensors is required.

Burned area data (30 m spatial resolution) can be obtained from operational meteorological and environmental satellites. In the optical regions: Multispectral Instrument (MSI) on-board Sentinel-2 and Operational Land Imager (OLI) onboard Landsat (e.g., Roy et al., 2019), complemented by Synthetic Aperture Radar (e.g., Sentinel-1) under cloudy conditions. Burned area can also be calculated based on observations from commercial operator satellites, just to mention Planet's high-resolution, analysis-ready mosaics of the world's tropics, which through Norway's International Climate & Forests Initiative (NICFI) can be assessed[13] (note: the purchased data cover the tropical forest, not the Arctic). Furthermore, burned area can be calculated from environmental satellites, e.g., NASA's Moderate Resolution Imaging Spectroradiometer (MODIS) aboard the Terra and Aqua satellites, NASA's Visible

---

[9] https://navigator.eumetsat.int/search?query=Active%20Fire%20Monitoring%20(CAP)%20-%20MSG%20-%200%20degree&filter=instrument__SEVIRI

[10] https://landsaf.ipma.pt/en/

[11] https://landsaf.ipma.pt/en/products/fire-products/frppixel/

[12] http://ane4bf-datap1.s3-eu-west-1.amazonaws.com/wmocms/s3fs-public/ckeditor/files/Space_Agency_Response_to_GCOS_IP_v2.2.1.pdf?NAb3qaxyu.kQg0Qw96xXSBXt1mGrxo.Q

[13] https://www.planet.com/nicfi/

Infrared Imaging Radiometer Suite (VIIRS) aboard the joint NASA/National Oceanic and Atmospheric Administration (NOAA) Suomi National Polar orbiting Partnership (Suomi NPP) and NOAA-20 satellites, and others. More details are given in Section 2.2.

Table 3: Validation Stage of fire ECV data (adapted from Duncanson et al., 2021, Table 1.2 CEOS validation stage hierarchy. The eventual goal is to mature existing and forthcoming biomass products from stage 0 to 4. [page 26, 27]).

Validation Stage - Definition and Current State		Variable
0	No validation. Product accuracy has not been assessed. Product considered beta.	
1	Product accuracy is assessed from a small (typically < 30) set of locations and time periods by comparison with in-situ or other suitable reference data.	Snow **Fire Radiative Power** Biomass
2	Product accuracy is estimated over a significant (typically > 30) set of locations and time periods by comparison with reference in situ or other suitable reference data. Spatial and temporal consistency of the product, and its consistency with similar products, has been evaluated over globally representative locations and time periods. Results are published in the peer-reviewed literature.	fAPAR Phenology **Burned Area** Land Cover LAI
3	Uncertainties in the product and its associated structure are well quantified over a significant (typically > 30) set of locations and time periods representing global conditions by comparison with reference in situ or other suitable reference data. Validation procedures follow community-agreed-upon good practices. Spatial and temporal consistency of the product, and its consistency with similar products, has been evaluated over globally representative locations and time periods. Results are published in the peer-reviewed literature.	Vegetation Indices Albedo Soil Moisture LST & Emissivity **Active Fire**
4	Validation results for stage 3 are systematically updated when new product versions are released or as the interannual time series expands. When appropriate for the product, uncertainties in the product are quantified using fiducial reference measurements over a global network of sites and time periods (if available).	

Vegetation fires burn with a wide range of temperatures, with flame radiative temperatures of about 700 K to 1500 K from smouldering to intense flaring combustion (Sullivan et al., 2003). Thus, they can be located by the thermal anomalies (**hot spots, active fire detection**) they produce. **FRP** is a measure of the energy released by the fire and is therefore a measure of how much vegetation is burned. Active fire data and FRP estimates can be obtained from MODIS, VIIRS, the Sea and Land Surface Temperature Radiometer (SLSTR), Landsat, and others. The data are distributed by e.g., NASA/NOAA, EUMETSAT and ESA (see Section 2.3 for more details).

FRP is directly proportional to the biomass burning rate (Wooster et al., 2005), so it can be used to determine fire emissions rates, considering land-use type specific **emission coefficients** (Andreae and Merlet, 2001, Akagi et al., 2011, Andreae et al., 2019). The needed **land cover** data can be obtained from several sites, e.g., from ESA Landcover_cci[14] or Copernicus C3S[15]. 500 m VIIRS land cover data[16] are available from the Land Processes Distributed Active Archive Center (LP DAAC, Zhang et al., 2020). See also the raster version of the 1-km Circumpolar Arctic Vegetation Map (CAVM[17], Raynolds et al., 2019) and the high resolution (10 m) land cover map for 2017 for Europe, including Norway, from Sentinel-2[18] (Gromny et al., 2019).

---

[14] https://www.esa-landcover-cci.org/

[15] https://cds.climate.copernicus.eu/cdsapp#!/dataset/satellite-land-cover?tab=overview

[16] https://lpdaac.usgs.gov/news/release-viirs-land-cover-dynamics-data-products/

[17] www.geobotany.uaf.edu, or

[18] https://s2glc.cbk.waw.pl/

2.2 Burned area datasets

The ESA Fire_cci[19] project aims to improve consistency, using better algorithms for both pre-processing and **burned area** detection while incorporating error characterisation. The following burned area products, which include Northern latitudes, are currently available:

- **FireCCI51**[20]: Fire_cci burned area dataset. It is based on MODIS data (global at 250 m and 0.25° for 2001 - 2020) (see Lizundia-Loiola et al., 2020)
- **FireCCILT11**[21]: Fire_cci long-term burned area dataset, going back to 1982. It is based on Advanced Very High Resolution Radiometer (AVHRR) and NASA/NOAA Land Long Term Data Record (LTDR) data (global at 0.05° and 0.25° for 1982 – 2018) (see Otón et al., 2021a, b)

For publications from the Fire_cci see: https://climate.esa.int/en/projects/fire/publications/. Recent publications deal with the validation approach for burned area products (Franquesa et al., 2020, 2022), and the transition from the FireCCI51 product based on MODIS to the Sentinel-3 Ocean and Land Colour Instrument (OLCI) product processed for the Copernicus Climate Change Service (C3S[22]) (Lizundia-Loiola et al, 2021).

NASA has developed a global burned area products based on MODIS.

- **MCD64A1**[23]: NASA's burned area dataset based on MODIS (global gridded, 500 m). It employs 500 m MODIS surface reflectance imagery coupled with 1 km active fire observations (see Giglio et al., 2018)

The FireCCI51 and MCD64A1, based on MODIS data, are the most accurate global products, widely used in different modelling studies (see the review by Chuvieco et al. (2019)). Chuvieco et al. (2019) lists satellite sensors used for burned area mapping (see *Table 4*) and overview of global burned area datasets (see Chapter 2.2).

Higher resolution data sets are not available globally, but on a continental-scale. See e.g., the continental-scale burned area data from Sentinel-2 for sub-Saharan Africa, developed in the Fire_cci (Roteta et al., 2019), and Sentinel-1 data are available for a demonstrator Area in the Amazon (Belenguer-Plomer et al., 2019).

Table 4: Satellite sensors used for burned area mapping (identical to Table 1, page 51, in Chuvieco et al. (2019))

Satellite (sensor)	Operator	Operational dates		Temporal resolution	Spatial resolution
		Launch date	End operation		
ENVISAT (MERIS)	ESA	March 1, 2002	May 9, 2012	2–3 days	300–1200 m
JPSS (VIIRS)	NOAA	October 28, 2011	Still operating	1–2 days	375–750 m
Landsat 1–3 (MSS)	NASA/USGS	July 23, 1972	September 7, 1983	18 days	80 m
Landsat 4–5 (TM)	NASA/USGS	July 16, 1982	June 5, 2013	16 days	30–120 m
Landsat 7 (ETM+)	NASA/USGS	October 5, 1993	Still operating	16 days	15/30–60 m
Landsat 8 (OLI/TIRS)	NASA/USGS	February 11, 2013	Still operating	17 days	OLI: 15/30 m TIRS: 100 m
NOAA-7-19 (AVHRR)	NOAA	Oct 19, 1978	Still operating	1–2 days	1100 m
PROBA V	ESA	May 7, 2013	Still operating	1–2 days	300 m
Sentinel 1A-B (SAR)	ESA	April 3, 2014 (1A) April 25, 2016 (1B)	Still operating	6 days	5–20 m
Sentinel 2A-B (MSI)	ESA	June 23, 2015 (2A) March 7, 2017 (2B)	Still operating	5 days	10–20–60 m
Sentinel 3A-B (SLSTR, OLCI)	ESA	16 February 2016 (3A) 25 April 2018 (3B)	Still operating	1–2 days	300 m OLCI, 500 m SLSTR
SPOT 1–7 (HRV)	CNES	February 22, 1986	Still operating	26 days	2.5 to 20 m
SPOT 4–5 (VGT)	CNES	March 24, 1998	July 2013	1–2 days	1000 m
Terra-Aqua (MODIS)	NASA	December 18, 1999 (Terra) May 4, 2002 (Aqua)	Still operating	1–2 days	250–1000 m

---

[19] https://climate.esa.int/en/projects/fire/

[20] https://geogra.uah.es/fire_cci/firecci51.php

[21] https://geogra.uah.es/fire_cci/fireccilt11.php

[22] https://climate.copernicus.eu/

[23] https://lpdaac.usgs.gov/products/mcd64a1v006/

Table 5: Overview of global burned area datasets (identical to Table 1, page 54, in Chuvieco et al. (2019))

Name of burned area dataset	Time span	Sensor/method	Spatial resolution g = grid p = pixel d = degree	Temporal compositing	Development purpose	Reference
GBA2000	2000	SPOT VGT	p:1 km, g:0.25 d, 0.5 d, 1 d	Monthly	Prototype	Tansey et al. (2004a, 2004b)
GLOBSCAR	2000	ERS2-ATSR2	p:1 km	Monthly	Prototype	Simon et al. (2004)
L3JRC	2000–2007	SPOT VGT	p: 1 km	Monthly	General purpose	Tansey et al. (2008)
GLOBCARBON	1998–2007	SPOT VGT, ATSR-2, AATSR	p: 1 km; g: 10 km, 0.25 d, 0.5 d	Monthly,	Global carbon cycling and climate models	Plummer et al. (2006)
GIO-GL1*	1999-present	SPOT VGT; from 04/2014 onwards: PROBA-V	p: 1 km	10-day composite	GHG reporting	Tansey et al. (2008)
GIO-GL1 300*	04/2014-present	PROBA-V	p: 300m	10-day composite	GHG reporting	
FireCCI41	2005–2011	Hybrid: MERIS reflectances guided by MODIS hotspots	p: 300m; g: 0.25 d	Monthly Biweekly	Climate and dynamic vegetation models	Chuvieco et al. (2016)
FireCCI50 and FireCCI51	2001–2017	Hybrid: MODIS reflectances guided by MODIS hotspots	p: 250m; g: 0.25 d	Monthly	Climate and dynamic vegetation models	Chuvieco et al. (2018) for FireCCI50
GFED4s	1997-present	Aug-2000 to present: MCD64A1 supplemented by small fire burned area (from scaled hotspots)	g: 0.25 d	Monthly with scalars for daily and 3-hourly estimations	Atmospheric and bio-geochemical models;	van der Werf et al. (2017)
GFED4	1995-present	Aug-2000 to present: MCD64A1 before: scaled ATSR or VIRS hotspots	g: 0.25 d	Monthly Daily (from Aug-2000)	Atmospheric and bio-geochemical models;	Giglio et al. (2013)
MCD45A1 c51	2000–01/2017	MODIS bi-directional reflectance (BRDF) temporal trends	p: 500m	Monthly	General purpose	Roy et al. (2008)
MCD64A1 c6	2000-present	Direct broadcast algorithm Hybrid: MODIS reflectances guided by MODIS hotspots	p: 500m; g: 0.25 d	Monthly	General purpose	Giglio et al. (2018)

2.3 Active fire and fire radiative power datasets

Landscape biomass burning typically involves radiating temperatures in the range of 700 K to 1500 K (Sullivan et al., 2003), with the peak of their spectral radiant energy emission occurring in or very close-to the middle infrared (MIR) spectral region. They produce a contrast when observed at different IR wavelengths, which made bi-spectral methods (Dozier, 1981) exploiting this, very interesting for fire detection (e.g., Giglio and Kendall, 2001), or the Planck-function fitting used in the VIIRS NightFire algorithm (Elvidge et al., 2013). Single band retrievals have an advantage in case of inter-channel spatial misregistration effects. Algorithms can be based on fixed thresholds, but nowadays they are replaced by self-adaptive, contextual fire detection schemes, where the spectral behaviour of a fire pixel is compared with the surrounding background. In *Table 6a,* and *6b*, satellite sensor characteristics for MODIS, VIIRS, SLSTS, Landsat, MSI, and Bi-spectral InfraRed Optical System (**BIROS**), all used for fire detection and/or parametrization, are summarized.

Table 6a: Comparison of satellite sensor characteristics used for fire detection and parametrization [adapted from Soszyńska (2022), Appendix A].

Sensor		MODIS	VIIRS	SLSTR
Name		Moderate Resolution Imaging Spectroradiometer	Visible Infrared Imaging Radiometer Suite	Sea and Land Surface Temperature Radiometer
Operated by		NOAA/NASA	NOAA/NASA	ESA/EUMETSAT
Orbit		705 km	829 km (828 -856 km)	786 km
Revisit time		1-2 days	0.5 day (both satellites)	0.5 day (both satellites)
Bands in VIS/NIR		yes	yes	yes
Spectral bands relevant for fire research	SWIR	B6 1.628 - 1.652 µm B7 2.105 - 2.155 µm	M10 and I3 1.58 - 1.64 µm M11 2.23 - 2.28 µm	S5 1.58-1.64 µm S6 2.23-2.28 µm
	MWIR	B20 3.660 - 3.840 µm B21 3.929 - 3.989 µm B22 3.929 - 3.989 µm B23 4.020 - 4.080 µm	I4 3.55-3.93 µm M12 3.61-3.79 µm M13 3.97-4.13 µm	S7 and F1 3.54-3.94 µm
	LWIR	B29 8.400 - 8.700 µm B30 9.580 - 9.880 µm B31 10.780 - 11.280 µm B32 11.770 - 12.270 µm	M14 8.4-8.7 µm M15 10.26-11.26 µm I5 10.5-12.4 µm M16 11.54-12.49 µm	S8 10.47-11.24 µm S9 and F2 11.57-12.48 µm
Ground sampling distance		250 m (bands 1–2) 500 m (bands 3–7) 1000 m (bands 8–36)	750 m for M-bands 375 m for I-bands	500 m (VIS-SWIR) 1000 m (MWIR-LWIR)
Field-of-View		110°	112.56°	68.5°
Swath		2330 km cross track 10 km along track at nadir	3060 km	1400 km nadir view 740 km along track view
Day-time - night-time images		Daytime Night-time	Daytime Night-time	Daytime (all bands) Night-time (only TIR)
Caveats		Large pixel size Age		F1, F2, increased dynamic range Saturation in all S7 BTs
Application		Detection Parametrisation	Detection Parametrisation	Detection Parametrisation

Table 6b: Comparison of satellite sensor characteristics used for fire detection and parametrization [adapted from Soszyńska (2022), Appendix A].

Sensor		OLI/Landsat-8*	MSI/Sentinel-2	BIROS[24]*
Name		Operational Land Imager	Multispectral Instrument	Bispectral InfraRed Optical Sensor
Operated by		NOAA/NASA	EUMETSAT	DLR
Orbit		705 km	786 km	500 km
Revisit time		16 days	5 days (both satellites)	5 days
Bands in VIS/NIR		yes	yes	yes
Spectral bands relevant for fire research	SWIR	SWIR1 1.56-1.66 µm SWIR2 2.1-2.3 µm	B11 1.568-1.659 (S2A) B11 1.563-1.657 (S2B) B12 2.115-2.290 (S2A) B12 2.093-2.278 (S2B)	
	MWIR			MWIR 3.4-4.2 µm
	LWIR	TIR1 10.6-11.2µm TIR2 11.5-12.5 µm		LWIR 8.6-9.4 µm
Ground sampling distance		100 m for TIR bands 30 m other	10 m (bands 2-4) 20 m (bands 5-8, 11, 12) 60 m (bands 1, 9, 10)	175 m (350 m)
Field-of-View		15°	20.6°	19.6° VIS-NIR, 19° IR
Swath		185 km	290 km	211 km VIS-NIR 178 km IR
Day-time - night-time images		Daytime (all bands) Night-time (only LWIR)	Daytime	Daytime Night-time
Caveats		Band saturation DN folding	Saturation	Suitable for analysis
Application		Active fire detection Burned area	Active fire detection Burned area	Detection Parametrisation
Comments		* use earlier instruments, and Landsat-9 OLI-2 (Masek et al., 2020)		*see Soszyńska (2022), and references therein

The BIROS satellite is the second of the FireBIRD[25] satellites (launched in July 2016), operated by the German Aerospace Center (DLR). It is a follow up of the Technology Experiment Carrier (TET-1[26]), launched July 2012, which was a predecessor of the Bi-Spectral Infrared Detection (**BIRD**) small satellite mission (Wooster et al., 2003) – the first small satellite mission for measuring temperature hotspots.

There is a long tradition for hot spots, active fire detection, and FRP estimates from **MODIS** (Kaufman et al., 1998, Justice et al., 2002, 2011, 2020, Giglio et al., 2003, 2006, 2016, 2020, Wooster et al., 2005, Peterson et al., 2013). Each MODIS active fire/thermal anomaly location represents the centre of a 1 km pixel that is flagged as containing one or more fires within the pixel. Since April 2021 MODIS Collection 6.1 has been available. Following MODIS fire products[27] are available:

MOD14/MYD14 v061	MODIS Terra/Aqua Thermal Anomalies/Fire 5-Minute L2 Swath 1 km
MOD14A1/MYD14A1 v061	MODIS Terra/Aqua Thermal Anomalies/Fire Daily L3 Global 1 km SIN Grid
MOD14A2/MYD14A2 v061	MODIS Terra/Aqua Thermal Anomalies/Fire 8-Day L3 Global 1 km SIN Grid

---

[24] https://www.dlr.de/content/en/articles/missions-projects/firebird/biros.html

[25] https://www.dlr.de/content/en/missions/firebird.html

[26] https://www.dlr.de/content/en/articles/missions-projects/firebird/tet-1.html

[27] https://modis.gsfc.nasa.gov/data/dataprod/mod14.php

Furthermore, the advanced spaceborne thermal emission and reflection radiometer (ASTER) (Giglio, et al., 2008), and **SEVIRI** (Roberts and Wooster, 2008), as well as **VIIRS** (Elvidge et al., 2013, Csiszar et al., 2014, Schroeder et al., 2014, Oliva and Schroeder, 2015) have been used for active fire detection and/or FRP. VIIRS active fire detection utilizing the 375 m image data provides improved performance compared to the 750 m product, with a theoretical minimum detectable night fire equivalent to ~ 5 m^2 and ~ 1000 K fire (Schroeder et al., 2014). Following VIIRS products[28] are available:

VNP14, VJ114	VIIRS NPP/JPSS1 6-Min L2 Swath 750m
VNP14IMG, VJ114IMG	VIIRS NPP/JPSS1 Active Fire 5-Min L2 Swath 375m
VNP14A1, VJ114A1	VIIRS NPP/JPSS1 Active Fire Daily L3 1km SIN Grid

SLSTR has two MWIR channels: S7 and F1 (dynamically enhanced) for land fire detection, and the SWIR channel S6 for flare detection (e.g., Wooster et al., 2012, Xu et al., 2020, KCL, 2019). A few active fire detection algorithms have been developed for higher resolution sensors such as Landsat-8 OLI images (Song et al. 2015, Murphy et al., 2016, Schroeder et al., 2016, Kumar and Roy, 2018, Kumar et al., 2020, Sofan et al., 2020) and Sentinel-2 MSI images (Dell'Aglio et al. 2019, Liu et al., 2021). FRP retrieval from these high resolutions is problematic due to saturation of the detector channels.

Data from European satellites are available in near real-time (NRT) from the EUMETSAT CODA system[29,30] and in non-time critical (NTC) format from the ESA Scihub[31]. The CreoDIAS[32] is an alternative data resource. NASA/NOAA data can e.g., be found via the LP DAAC[33]. NASA's Fire Information for Resource Management System (FIRMS[34]) provides NRT global fire/thermal anomaly maps and data within 3 hours of satellite observation from MODIS (Aqua/Terra) and VIIRS (Suomi NPP, NOAA-20). Email alerts with notifications of fires in an area-of-interest are provided. The NRT data are replaced with data extracted from the standard MODIS and VIIRS active fire products after they becomes available (usually after 2-3 months) ["archive download"]. VIIRS Nightfire (VNF) nightly data are produced by the Earth Observation Group, Payne Institute for Public Policy, Colorado School of Mines, and are made available for scientific non-profit users without charge (data license agreement needed).

---

[28] https://lpdaac.usgs.gov/product_search/?query=VIIRS&view=cards&sort=title

[29] https://navigator.eumetsat.int/product/EO:EUM:DAT:0207

[30] https://www.eumetsat.int/coda

[31] https://scihub.copernicus.eu/

[32] https://creodias.eu/

[33] https://lpdaac.usgs.gov/

[34] https://earthdata.nasa.gov/earth-observation-data/near-real-time/firms

2.4 Aerosol (AAI, and other) and trace gas (CO) smoke plume tracer

Many satellite sensors measure aerosols, which provide data regularly used for monitoring of aerosol layers from wildfires, such as data from e.g., MODIS[35], VIIRS[36], SLSTR (NRT data from EUMETSAT[37], and as NTC data from ESA[38]), and the Cloud-Aerosol Lidar with Orthogonal Polarization (CALIOP[39,40]) on the Cloud-Aerosol Lidar and Infrared Pathfinder Satellite Observations (CALIPSO). Data from the latter have frequently been used for identification plumes transported towards Ny-Ålesund, and for validation of transport modelling of fire and other pollution episodes, like dust events.

For tracking smoke plumes using satellite observations, parameters such as Carbon Monoxide (CO) and Aerosol Absorbing Index (AAI) are particularly useful. CO is emitted from incomplete combustion and has an atmospheric lifetime of a few weeks to several months and is mainly removed by OH. The aerosol index was originally defined for the correction of aerosols in total ozone measurements made by the Total Ozone Mapping Spectrometer (TOMS) instruments (Herman et al., 1997; Torres et al., 1998). AAI is a qualitative indicator of the presence of UV absorbing aerosols (Ginoux, Torres and Torres, 2003).

Different web-based services offer quicklooks of these parameters: NRT images (including calendar for earlier dates) are accessible from the Support to Aviation Control Service (SACS[41]), which is hosted by the Royal Belgian Institute for Space Aeronomy (BIRA-IASB). SACS provides quick looks for AAI from GOME-2 and UVAI from TROPOMI. UVAI NRT quick-looks from the Ozone Monitoring Instrument (OMI) onboard AURA and the Ozone Mapping and Profiler Suite (OMPS) onboard Suomi-NPP are also provided by the Satellite Measurements from Polar Orbit (SAMPO[42]) service from the Finnish Meteorological Institute (FMI). GOME-2 AAI can be downloaded from the FMI Satellite Application Facility on Atmospheric Composition Monitoring (AC SAF[43]). Infrared Atmospheric Sounding Interferometer (IASI) CO quicklooks can be found on the AERIS data hub[44]. TROPOMI UVAI and CO can be downloaded from the Sentinel 5P pre-operations data hub[45]. Quicklooks can be found on the Sentinel EO browser[46].

---

[35] https://modis.gsfc.nasa.gov/data/dataprod/mod04.php
[36] https://earthdata.nasa.gov/earth-observation-data/near-real-time/download-nrt-data/viirs-a-nrt
[37] https://navigator.eumetsat.int/product/EO:EUM:DAT:0306
[38] https://apps.sentinel-hub.com/eo-browser
[39] https://www-calipso.larc.nasa.gov/products/
[40] https://asdc.larc.nasa.gov/
[41] https://sacs.aeronomie.be/nrt/
[42] www.sampo.fmi.fi
[43] https://acsaf.org/
[44] https://iasi.aeris-data.fr/
[45] https://s5phub.copernicus.eu/dhus/#/home
[46] https://apps.sentinel-hub.com/eo-browser

3 CAMS and CEMS

The European Centre for Medium-Range Weather Forecasts (ECMWF[47]) provides **monitoring** and **forecasting** of global wildfire emissions and danger conditions through the Copernicus Emergency Management Services (**CEMS**) and the Copernicus Atmosphere Monitoring (**CAMS**), linking fire forecasts to pollution concentration and emissions. CEMS provides information for emergency response in relation to different types of disasters. The following four models contribute to CEMS: 1. Emergency Mapping, 2. European and Global Flood Awareness System, 3. European Forest Fire Information System (EFFIS), and 4. the European Drought Observatory. CEMS forecasts global fire danger with the Global ECMWF Fire Forecasting (GEFF) model. Daily forecasts are available via CEMS **EFFIS** (for Europe) and **GWIS** (globally). CAMS provides products for monitoring global fire emissions and atmospheric impacts. The CAMS global production system is the ECMWF Integrated Forecast System (IFS), which is a full Numerical weather prediction (NWP) forecasting and data assimilation system of ECMWF.

3.1 Global Wildfire Information System

The **Global Wildfire Information System (GWIS[48])** is a is a joint initiative of the Group on Earth Observations (GEO[49]) and the Copernicus emergency[50] work programme (CEMS) and is supported by NASA. GWIS brings together information sources at the regional and national level on fire regimes and effects and provides tools for operational wildfire management from national to global scales, e.g., landcover (CCI[51] maps) and fuels. Country maps and country-specific charts for a variety of fire related parameter, i.e., burned area, number of fires and emission, are provided. GWIS uses the active fire detections provided by the NASA's Fire Information for Resource Management System (FIRMS[52]) for active fires from MODIS and VIIRS. FIRMS is part of the NASA Earth Observing System Data and Information System (EOSDIS). The MODIS MOD64A1 Collection 6 Burned Area product (Giglio et al., 2018) is used to create country-level burned area statistics. At present, data from 2001 to February 2018 are available.

The GWIS Current Situation Viewer[53] provides NRT information on fire danger forecast, lightning occurrence, MODIS and VIIRS active fire detection and burned area perimeters, and CAMS fire emissions. The Current Statistics Portal provides statistic at national level and for regions of interest, e.g., for the Arctic Monitoring and Assessment Program (AMAP). Country Profile information of fire regimes for the period 2002 onwards is given. *Figure 2* shows the actual GWIS country profile for Norway. Furthermore, the Long-term fire weather forecast provides monthly and seasonal global forecast of temperature and rainfall anomalies. Data used in the GWIS applications, can be downloaded[54].

---

[47] https://www.ecmwf.int/
[48] https://gwis.jrc.ec.europa.eu/
[49] https://www.earthobservations.org/index.php
[50] https://www.copernicus.eu/en/services/emergency
[51] https://www.esa-landcover-cci.org/
[52] https://earthdata.nasa.gov/earth-observation-data/near-real-time/firms
[53] https://gwis.jrc.ec.europa.eu/apps/gwis_current_situation/
[54] https://gwis.jrc.ec.europa.eu/applications/data-and-services
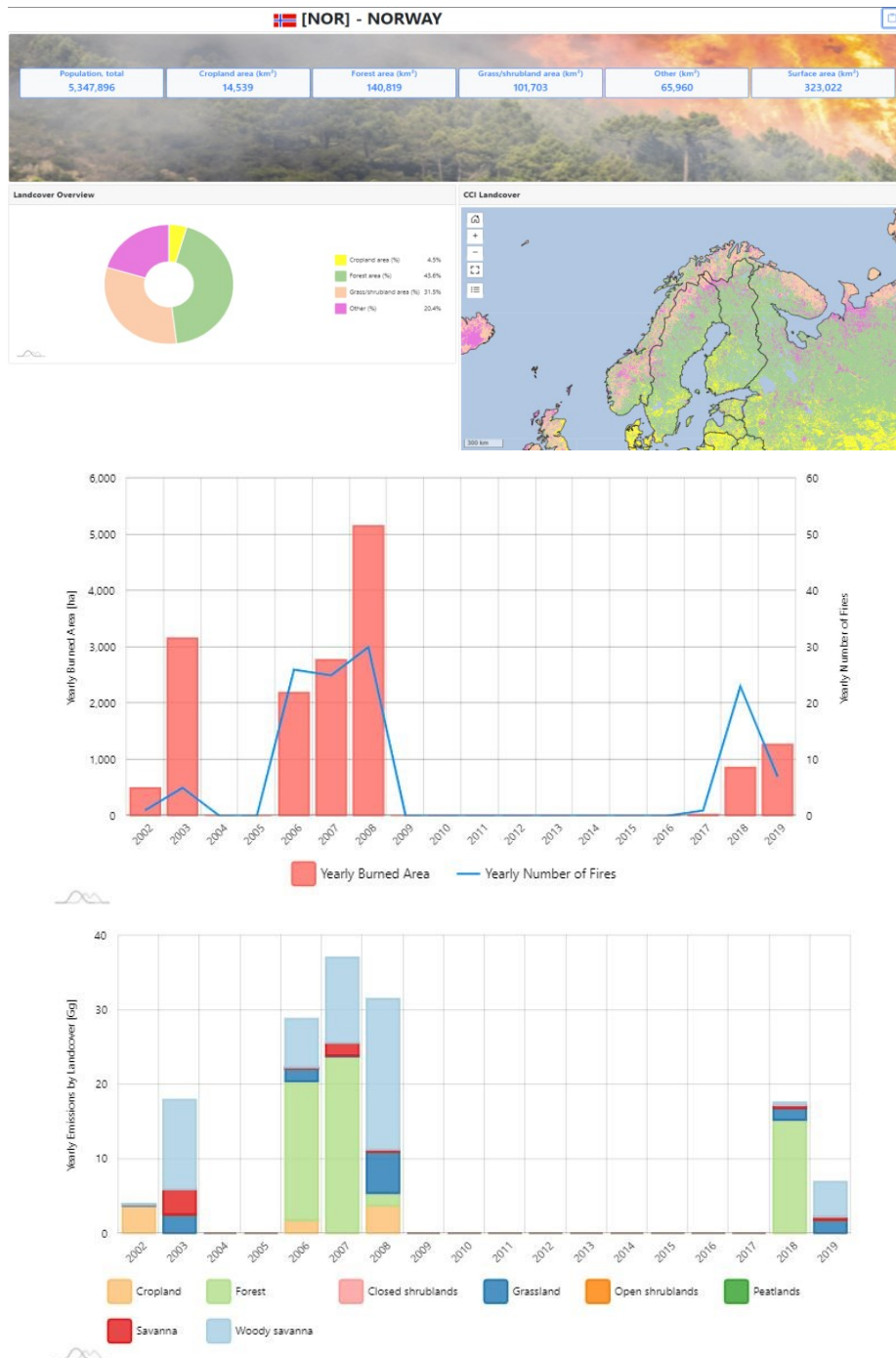
Figure 2: GWIS country profile for Norway. Upper panels: Country profile and landcover; middle panel: yearly burned area and number of fires; lower panel: Yearly carbon dioxide (CO_2) emissions by landcover (both for 2002-2019).

Examples of maps from GWIS are shown in *Figure 3*, illustrating the Arctic wildfire in Russia in 2019. Daily total wildfire emissions were well above the 2003 - 2018 average throughout the summer north of the Arctic Circle. Many wildfires were concentrated in the Sakha Republic, Russia with other fire activity in Alaska, Yukon Territory and Greenland. *Figure 4* gives an overview over wildfires in the Arctic in the period from 2015 to 2020. Emissions in 2020 were topping the one from the previous year.
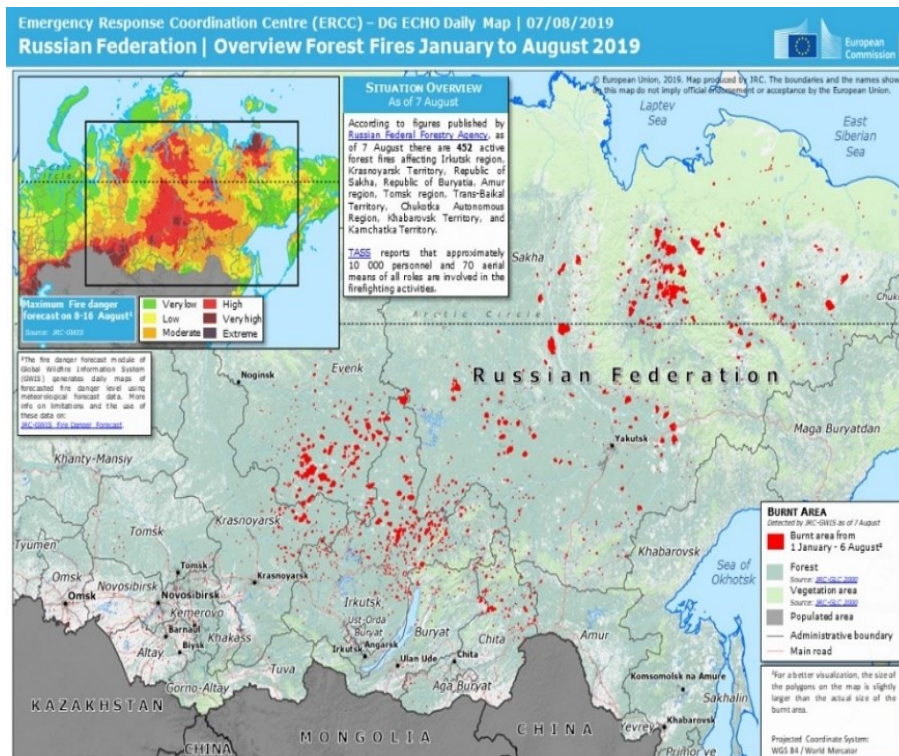
Figure 3: GWIS maps showing and overview over forest fire in Russia in January to August 2019[55]
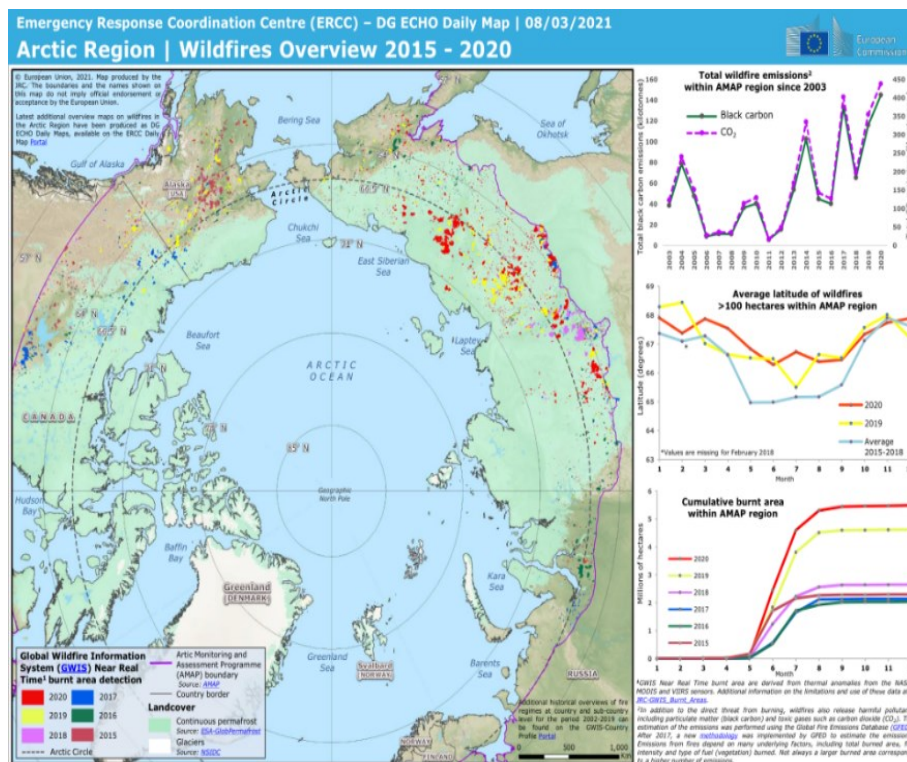
Figure 4: GWIS maps showing an overview over wildfires in the Arctic in 2015 – 2020[56].

---

[55] https://effis-gwis-cms.s3-eu-west-1.amazonaws.com/gwis/reports-and-publications/ercc-daily-map/20190807_Forestfires_Russia.png

[56] https://effis-gwis-cms.s3-eu-west-1.amazonaws.com/gwis/reports-and-publications/ercc-daily-map/20210308_Arctic_ForestFires_Emissions.png

3.2 The European Forest Fire Information System - Norway country report

The **European Forest Fire Information System (EFFIS**[57]**)**, which is managed by the Joint Research Centre (JRC), provides NRT and historical information on forest fires and forest fire regimes in the European, Middle Eastern and North African regions. Since 2015 it is one of the three early warning component of the Copernicus Emergency Management Service (CEMS[58]). ECMWF is the computational centre for EFFIS.

EFFIS makes a few specific applications available via their webpage. A current situation viewer shows e.g., today meteorological fire danger maps and forecast up to 6 days, active fires and burned area (based on VIIRS and MODIS data). The statistical portal provides information accumulated on country level, including statistics on burned area and number of fires, seasonality, and trends. It also includes number of thermal anomalies detected by VIIRS and MODIS. Furthermore, fire news is collected and can be selected according to country. Note that no reports were found for Norway. In addition, monthly and seasonal forecasts of fire weather, country totals (burned areas & number of fires) per year are given, as well as a form for additional data requests.

Also note a related data resource in the Copernicus climate data store (**CDS**), such as the gridded (0.11° x 0.11°) **Fire Weather Index** (**FWI**[59]) for Europe, which is produced on behalf of the Copernicus Climate Change Service. The dataset presents projections of fire danger indicators for Europe based upon the Canadian Fire Weather Index System under future climate conditions. Fire weather indicators from 1970 to 2018 are derived from reanalysis and climate projections. They include the number of days with moderate, high, or very high fire danger conditions as classified by the European Forest Fire Information System (EFFIS) during the northern hemisphere's fire season (June-September).

EFFIS is supported by an Expert Group on Forest Fires[60], which consists of experts from 43 countries in European, Middle East and North African countries. The group supports the European Commission to review forest fire trends in Europe and to determine adequate and effective responses. The Norwegian **Directorate for Civil Protection** (**DSB**[61], C. A. Hornstuen) is an Observer in the Expert Group on Forest Fires. DSB is responsible for the populations and fire services through laws and regulations, maintains the system for statistical reporting of fires (Brann, Redning, Innrapportering, Statistikk (BRIS) "Fire, Rescue, Reporting, Statistics"), facilitates the Norwegian Forest Fire committee (Members: DSB, Fire Services, The Norwegian Meteorological Institute, Insurance, Areal resources, and Fire Associations), and participated in the Nordic working group for wildland fires, a new European reserve of resources (rescEU-team[62]). For Norway, the **Norwegian Meteorological Institute** (**MET**) performs calculations of the **forest fire hazard index** (Waldbrannkennziffer, WBKZ). Forest fire warnings are issued on a regular basis during the snow-free "summer season" from April onward. The fire index is calculated based on around 100 places in the country. WBKZ is a cumulative index, based on precipitation, air temperature and humidity observations, the latter two parameter determining the degree of dryness in the air. Because WBKZ can be low biased after precipitation, the adaptation of a new common forest fire danger index is under evaluation by the Nordic weather services (DSB, 2019).

---

[57] https://effis.jrc.ec.europa.eu/

[58] https://www.copernicus.eu/en/copernicus-services/emergency

[59] https://climate.copernicus.eu/fire-weather-index

[60] https://ec.europa.eu/transparency/regexpert/index.cfm?do=groupDetail.groupDetail&groupID=416

[61] https://www.dsb.no/

[62] https://ec.europa.eu/echo/what/civil-protection/resceu_en/

EFFIS provides annual reports on forest fires in Europe (San-Miguel-Ayanz et al., 2021), including country reports for Norway. The new announcement[63] from 22 March 2022, informs about that the EU 2021 wildfire season was the second worst on record. Trends regarding both the number of fires and burned areas from 2000-2020 as given by Botnen (2021) are shown in *Figure 5*. According to the 2020 country report for Norway (Botnen, 2021) 609 fires were registered in 2020, which is 291 % of the 2010 - 2019 average (209 fires), and 363 ha burned area, equivalent to 34% of the 2010-2019 average (1068 ha burned area). The most recent information from EFFIS is given in the preliminary report on the 2021 fire campaign (San-Miguel-Ayanz, 2022). The data for Norway are shown in *Figure 6*. In 2021 991 ha from 22 fires were burned.

According to Botnen (2021), in Norway, most forest fires are man-made, followed by lightning/thunderstorms. The fire season lasts normally from March to September. It starts in the south-west in March/April and during the season it moves south- and eastward. In the west we see mainly bush-fires, whereas pines burn in the southern part. Norway's largest forest areas are in the south-east of the country. In Norway, more extreme events are expected as results of climate change, with more precipitation, but also increasing temperatures and droughts. One of the consequences can be that dry areas become even drier. Furthermore, it can imply increase growth in grass, shrubs, and trees, overgrowing of cultural landscapes, thus a longer fire season and larger fires as a result of more fuel (Botnen, 2021).
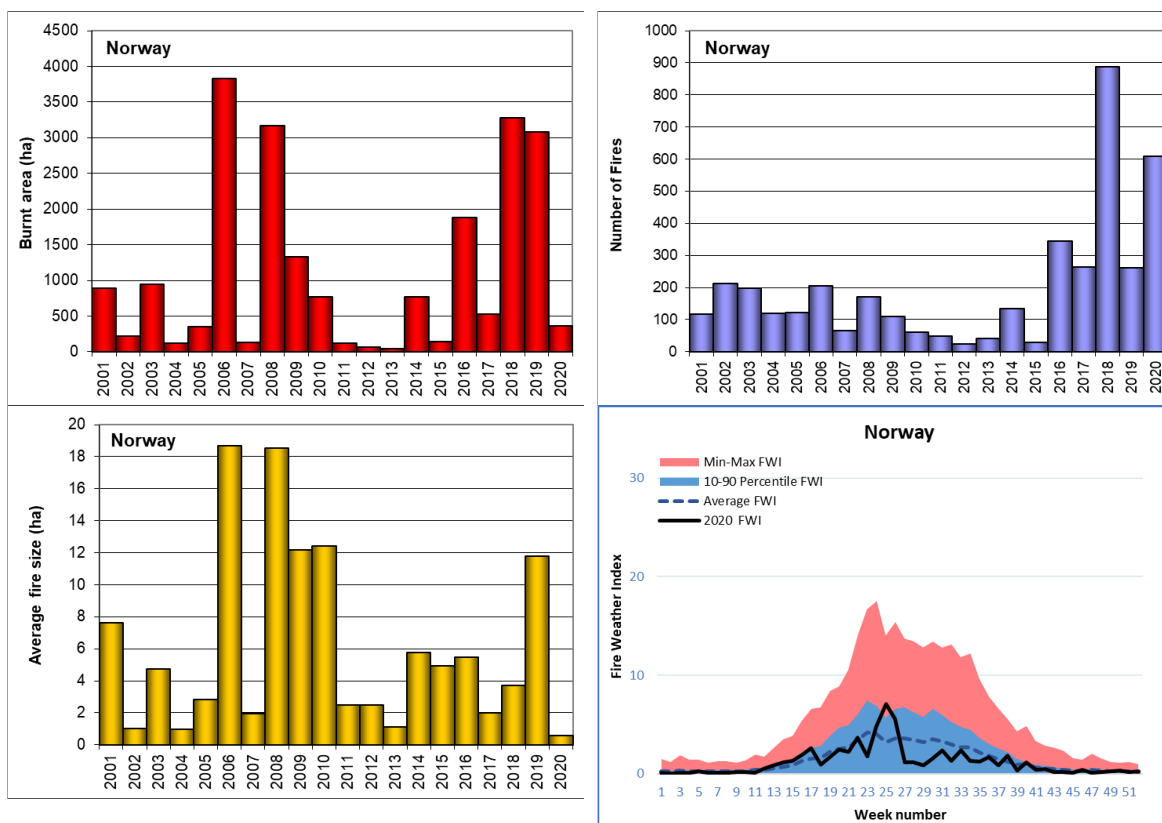
Figure 5: Adapted from Botnen (2021) [Figure 64 on page 59] Upper left panel: burned areas, upper right panel: number of fires, lower left panel: average fire size in Norway from 2001 to 2020. Lower right panel: [equal to Figure on page 136]: EFIS Danger Forecast, Red: extreme values in period 1980-2020, blue: 10-90th percentile, dotted: long term average (1080-2020), solid: 2020 values.

---

[63] https://joint-research-centre.ec.europa.eu/jrc-news/eu-2021-wildfire-season-was-second-worst-record-finds-new-commission-report-2022-03-21_en

1.3.21 Norway

There were fires mapped in Norway from March to August, resulting in a total of 991 ha from 22 fires. Most of the damage occurred early in the season, in April and June. Other Natural Land was the land cover type most affected, as shown in Table 23.

Table 23. Distribution of burnt area (ha) in Norway by land cover types in 2021.

Land cover	Area burnt	% of total
Broadleaf forest	43	4.4
Coniferous forest	23	2.3
Mixed forest	55	5.6
Other Natural Land	859	86.7
Agriculture	9	0.9
Other Land Cover	2	0.2
TOTAL	**991**	**100**
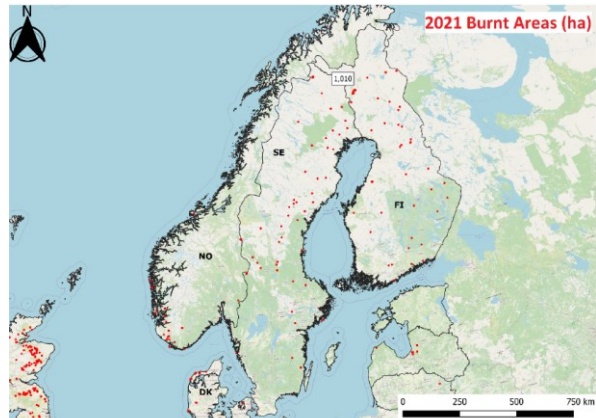
Figure 15. Burnt area scars in Scandinavia in 2021. Largest fire is indicated in ha.
NO=Norway; SE=Sweden; FI=Finland; DK=Denmark.

Figure 6: Most recent information from EFFIS for the year 2021. Left panel: equal to Table 23 [on page 24]; right panel: equal to Figure 15 [on page 20] in San-Miguel-Ayanz et al. (2022).

3.3   Global Fire Assimilation System and other fire emission inventories

The Copernicus Atmosphere Monitoring Service (CAMS) **Global Fire Assimilation System (GFAS**[64], for GFASv1.2, see Kaiser et al., 2012) assimilates satellite fire radiative power (FRP) observations from Aqua and Terra MODIS (https://modis-fire.umd.edu/) to produce global daily estimates of emissions of pollutants from wildfires and biomass burning. The spatial resolution is of 0.1° on a regular latitude - longitude grid. Data cover the period from 2003 to present and are released one day behind NRT. Emissions of aerosols and gases are estimated using factors dependent on vegetation type.

Table 7 shows the numerous wildfire related parameter, which can be downloaded[65] from GFAS. Latest CAMS 5-day global forecasts visualized via website and selected parameter are visualized on the mobile app of windy.com, e.g., fire intensity[66] or CO concentration[67].

Table 7: List of data provided by GFAS.

- Altitude of plume bottom
- Altitude of plume top
- Injection height (from IS4FIRES)
- Mean altitude of maximum injection
- Wildfire combustion rate
- Wildfire flux of acetaldehyde (C_2H_4O)
- Wildfire flux of acetone (C_3H_6O)
- Wildfire flux of ammonia (NH_3)
- Wildfire flux of benzene (C_6H_6)
- Wildfire flux of black carbon
- Wildfire flux of butanes (C_4H_{10})
- Wildfire flux of butenes (C_4H_8)
- Wildfire flux of carbon dioxide (CO_2)
- Wildfire flux of carbon monoxide (CO)
- Wildfire flux of dimethyl sulfide (DMS) (C_2H_6S)
- Wildfire flux of ethane (C_2H_6)
- Wildfire flux of ethanol (C_2H_5OH)
- Wildfire flux of ethene (C_2H_4)
- Wildfire flux of formaldehyde (CH_2O)
- Wildfire flux of heptane (C_7H_{16})
- Wildfire flux of hexanes (C_6H_{14})
- Wildfire flux of hexene (C_6H_{12})
- Wildfire flux of higher alkanes (CnH_{2n+2}, c>=4)
- Wildfire flux of higher alkenes (CnH_{2n}, c>=4)
- Wildfire flux of hydrogen (H)
- Wildfire flux of isoprene (C_5H_8)
- Wildfire flux of methane (CH_4)
- Wildfire flux of methanol (CH_3OH)
- Wildfire flux of nitrogen oxides (NOx)
- Wildfire flux of nitrous oxide (N_2O)
- Wildfire flux of non-methane hydrocarbons
- Wildfire flux of octene (C_8H_{16})
- Wildfire flux of organic carbon
- Wildfire flux of particulate matter d < 2.5 μm (PM2.5)
- Wildfire flux of pentanes (C_5H_{12})
- Wildfire flux of pentenes (C_5H_{10})
- Wildfire flux of propane (C_3H_8)
- Wildfire flux of propene (C_3H_6)
- Wildfire flux of sulphur dioxide (SO_2)
- Wildfire flux of terpenes (($C_5H_8)n$)
- Wildfire flux of toluene (C_7H_8)
- Wildfire flux of toluene_lump (C_7H_8+ C_6H_6 + C_8H_{10})
- Wildfire flux of total carbon in aerosols
- Wildfire flux of total particulate matter
- Wildfire flux of xylene (C_8H_{10})
- Wildfire fraction of area observed
- Wildfire overall flux of burnt carbon
- Wildfire radiative power

---

[64] https://www.ecmwf.int/en/forecasts/dataset/global-fire-assimilation-system

[65] http://apps.ecmwf.int/datasets/data/cams-gfas/

[66] https://www.windy.com/-Show---add-more-layers/overlays?fires,59.933,10.898,5

[67] https://www.windy.com/-Show---add-more-layers/overlays?cosc,59.933,10.898,5

The Global Fire Emissions Database **GFED**[68] is produced by the Vrije Universiteit Amsterdam, cluster Earth and Climate, GFEDv4s is a most recent version of fire emissions derived from satellite burned area products (van der Werf et al., 2017). Earlier versions are GFEDv2 (van der Werf et al., 2006), and GFEDv3 (van der Werf et al., 2010). Data (burned area, monthly emission and fractional contribution of different fire types, daily/3-hourly fields to scale the monthly emissions to higher temporal resolutions) from 1997 onward are provided. Mapped burned area are without small fires (GFEDv4 burned area based on retrieval by Giglio et al., 2013). The Global Fire Emissions Database with small fires (**GFEDv4s**; van der Werf et al., 2017) integrates the MODIS burned area product with the active fire product to account for small fires (Giglio et al., 2009). See also the Global Fire Atlas[69] of individual fire size, duration, speed, and direction, by Andela et al. (2019), which is based on the 500 m resolution MODIS (MCD64A1 collection 6) daily burned area product.

Further inventories to mention are e.g., the Fire inventory from National Center for Atmospheric Research (NCAR) (**FINN**[70], Wiedinmyer et al., 2011, Wiedinmyer et al., 2023), the high-resolution Quick Fire Emissions Dataset (**QFED**, Darmenov and da Silva, 2015, Koster et al., 2015), and NASA's Fire Energetics and Emissions Research (**FEER**, Ichoku and Ellison, 2014). For a comparison of biomass emission data sets with respect to aerosol modelling, see Pan et al., (2020).

Fire emissions data can be visualized and downloaded from the Regional Evaluation, Comparison, and Metrics (**FIRECAM**[71]) Tool, which is an Earth Engine App, online app for end-users to diagnose and explore regional differences in fire emissions from five global fire emissions inventories (GFEDv4s, FINNv1.5, GFASv1.2, QFEDv2.5r1, FEERv1.0-G1.2) (Liu, 2020).

---

[68] https://www.globalfiredata.org/
[69] https://www.globalfiredata.org/fireatlas.html
[70] https://www2.acom.ucar.edu/modeling/finn-fire-inventory-ncar
[71] https://sites.google.com/view/firecam/home

4   Knowledge gaps and limitations of satellite remote sensing

McCarty et al. (2021) summarize knowledge gaps and uncertainties in understanding Arctic fire regimes and emissions. The authors discuss open questions and give recommendations related to spatial and temporal modelling of future fire landscapes and regimes, peatlands, permafrost, and satellite-based fire emissions.

Fire activity data are derived from ground- and satellite-based sources. For global inventories, satellite-derived fire activity is estimated by active fire detections, burned area mapping, and fire radiative power. Availability of satellite-derived fire activity of good quality, as well as knowledge of emission factors and fuels, determine the quality and uncertainties in fire emission model inventories (e.g., Liu et al., 2020, Pan et al., 2020).

Many of the present fire emission inventories are based on MODIS data only, which can lead to underestimation of burned areas, particular in agricultural landscapes. Zhu et al. (2017) compared the MODIS burned area product with higher-resolution (better than 30 m) satellite products as a reference. They found that MODIS burned area comprised only 13% of the reference products in croplands because of inadequate detection of small fires (<100 ha). Another uncertainty aspect to mention is that surface fires, that burn under canopies, dominate fire regimes in Northern Eurasia, and these burned areas are not currently accurately quantified (Duncan et al., 2020). Thus, understanding the balance between surface-to-crown fire is important.

Hold-over fires, which can be spread out underground, are not so easy to spot and characterize. In smouldering the heat release occur on the surface of the solid, whereas in flaming combustion it occurs in the gas phase (Rein et al., 2008). Smouldering fires have comparable low temperatures and spread rate (500 – 700°C, 0.1 – 5 cm per hour) compared to flaming combustion (around 1500°C, 10 m per hour) (Drysdale, 1998). They can burn underground, re-appear at different locations and/or time (Rein, 2016). Johnston et al. (2018) found that satellite instruments with pixel sizes around 375 m (e.g., as offered by the VIIRS I-Bands) can detect canopy smouldering fires throughout the North American boreal forests down to a size of 0.2 ha. Instruments with larger pixel size, e.g., MODIS and SLSTR (MIR: 1 km at nadir), are only able to detect a 0.2 ha fire in northern latitudes where forest canopies (and human populations) are less dense (Johnston et al., 2018).

McCarty et al. (2021) also point out the lack of agreement between official statistics and satellite observations. Norway generally has low fire activity and burned area. McCarty et al. (2021) showed that GWIS satellite-derived burned area, which is based on MODIS (Giglio et al., 2018), overestimated open biomass burning in Norway in 2019 (0.03 km^2 according to DSB (2020)) by 199%. Fusco et al. (2019) conclude that satellite data are less likely to align with official records as fire sizes decrease. The detection of small fires is essential for a better agreement between burned area products in several regions (e.g., Randerson et al., 2012; Mangeon et al., 2015), particularly for fire due to agricultural waste burning (Chuvieco et al., 2016, 2019).

Generally, satellite products suffer from ignoring fires burning under clouds. Retrieval omission and commission errors need to be known. One of the main challenge is to discriminate between permanent sources of heat (bright surfaces, gas fares, etc.) and fire events. Fire shows a very strong diurnal cycle, which must be considered when developing long-term datasets from multiple missions, that may have different local overpass times and can have varying sensitivity, lower/upper detection limits. Data continuity is an important aspect for future operational satellites. Ground-level verification, intercomparison and combination of data is essential to get the best estimate of fire occurrence and their emissions, including uncertainty estimates over long timescales.

5   Future missions

The two **MetOp-Second Generation satellites** (MetOp-SG[72]) form the space segment of the EUMETSAT Polar System Second Generation (EPS-SG). **MetOp-SG[73]-A** will be launched into a sun-synchronous orbit earliest in summer 2024, carrying eight instruments. For fire related information, the following are relevant: the METimage (DLR), the Infrared Atmospheric Sounder Interferometer-Next Generation (IASI-NG) (CNES), the Multi-view Multi-channel Multi-polarization Imager (3MI) (ESA), Sentinel-5[74]/UVNS (ESA/Copernicus) and the Low Light Imager (NOAA).

The **METimage** will provide continuity and great improvement with respect to AVHRR, and comparable performance to VIIRS. Besides other products (e.g., clouds, aerosols, sea surface temperatures, vegetation), it will provide fire monitoring products. It covers a broad spectral range in 20 spectral bands from 443 nm to 13.345 µm, including SWIR and MWIR bands at 1.63 µm (VII-24), 2.25 µm (VII-25), 3.74 µm (VII-26) 3.959 µm (VII-28) 4.05 µm (VII-30) suitable for **fire detection and quantification**.

IASI-NG, 3MI, and UVNS will provide **trace gas and aerosol measurements** suitable for **tracking emissions from fires**. IASI-NG will measure several relevant trace gas measurements like O_3, CO_2, CO, SO_2, CH_4, HNO_3, NH_3 and NO_2. 3MI will provide a multi-spectral (from 410 to 2130 nm), multi-polarisation (−60°, 0°, and +60°), and multi-angular (14 views) image of the Earth outgoing radiance at the top of the atmosphere for high quality imagery of aerosols variables for climate records. UVNS on Sentinel-5 will provide hyper-spectral soundings with a spectral resolution from 0.065 −1 nm in the wavelength ranges from 0.27–2.4385 µm, at a spatial sampling of 7 km for channels above 0.3 µm. It will measure O_3 profiles and total column, SO_2, NO_2, water vapour, CH_4, CO_2, CO, BrO, HCHO, OCHCHO, and volcanic plumes. Finally, using a photomultiplier tube, the VIS signal is enhanced at night, making it possible to **detect** low emissions from lights, **fires**, lava flows, and gas flares.

The ESA's Earth Clouds, Aerosols and Radiation Explorer (**EarthCARE**[75]) will be earliest launched in September – mid October 2023 (depending on availability of a launcher, delays are anticipated). EarthCARE will carry four instruments: the Atmospheric Lidar (ATLID), the Cloud Profiling Radar (CPR), the Broad-Band Radiometer (BBR), and the Multi-Spectral Imager (MSI). ATLID will provide vertical profiles of aerosols and thin clouds, CPR will measure vertical profiles measurements of clouds, as well as vertical velocities of cloud particles. BBR will do measurements of top-of-the-atmosphere radiances and fluxes, and MSI will measure clouds and aerosols with channels in the VIS, NIR, SWIR and TIR. EarthCARE will enable horizontal and vertical tracking of smoke plumes and the estimation of their **radiative impacts**.

Further missions interesting in relation to fires are ESA's forest mission **Biomass[76],** with launch planned in late 2023. Biomass will carry a novel P-band synthetic aperture radar. The mission will give information about the state and change of **forests** and their role in the carbon cycle. ESA's FLuorescence EXplorer (**FLEX**[77]) will carry the high-resolution Fluorescence Imaging Spectrometer (FLORIS), which will acquire data in the 500 - 780 nm spectral range. The launch is planned for summer 2025. Potential utilization of the potassium emission line signature for the detection of **flaming combustion** (e.g., Vodacek et al., 2002) is under evaluation.

---

[72] https://directory.eoportal.org/web/eoportal/satellite-missions/m/metop-sg
[73] https://www.eumetsat.int/metop-sg
[74] https://sentinels.copernicus.eu/web/sentinel/missions/sentinel-5
[75] https://earth.esa.int/eogateway/missions/earthcare
[76] https://www.esa.int/Applications/Observing_the_Earth/FutureEO/Biomass
[77] https://earth.esa.int/eogateway/missions/flex

6   User uptake and user groups

Fires are relevant for many entities in Norway, including the relevant authorities, institutions with operational tasks, researchers from the institute sector and universities working on fire related aspects. Furthermore, information about fires is of relevant for the public, as well for media and other interested entities (e.g., insure companies, companies in forestry, energy sector, …). The main actors are:

The **Norwegian Directorate for Civil Protection** is an Observer in the Expert Group on Forest Fires[78], which supports EFFIS. DSB is responsible for the populations and fire services through laws and regulations, maintains the system for statistical reporting of fires (BRIS), facilitates the Norwegian Forest Fire committee (Members: DSB, Fire Services, The Norwegian Meteorological Institute, Insurance, Areal resources, and Fire Associations), and participated in the Nordic working group for wildland fires. The **Norwegian Environmental Agency** is responsible for the air quality reporting to the EU/European Commission. The **Norwegian Meteorological Institute** performs calculations of the forest fire hazard index and issues information/warnings. The **Norwegian Institute of Bioeconomy Research (NIBIO)** Division of Forestry and Forest Resources is responsible for the National Forest Inventory, as well as the preparation of national forest statistics and forecasts for forest resources. The **Norwegian Institute for Air Research (NILU)** is responsible for monitoring of long-range transported air pollutions, GHG's and aerosols on commission of the Norwegian Environmental Agency. NILU contributes to the AMAP Expert Group on Short-Lived Climate Forcers (AMAP, 2021, review on Arctic fires by Mc McCarty et al., 2021).

The **Center for International Climate Research (CICERO)** has interdisciplinary climate research in focus. CICERO contributes e.g., to reduce climate change induced health impacts of air-pollution, heatwaves, and wildfires in Europe (EU project EXHAUSTION[79]), or ACRoBEAR[80] (Arctic Community Resilience to Boreal Environmental Change: Assessing Risks from fire and disease), funded by the Belmont Forum. Wildland-Urban Interface (WUI[81]) Fire Risk is an ongoing research project at the **Western Norway University of Applied Sciences (HVL)**. The goal of the project is to prevent devastating WUI fires in the *Calluna vulgaris* (heather) dominated Norwegian landscape. The project shall develop risk warnings and support civic groups working to reduce the WUI fire risk in coastal Norway. The main objective of the **Fire Research and Innovation Centre** (**FRIC**[82]) is to increase knowledge within the field of fire science to support decisions and develop better solutions providing increased fire safety in buildings. FRIC started in spring 2019 and is funded by the Research council in Norway. It is led by RISE Fire Research[83] in Trondheim, with **Norwegian University of Science and Technology (NTNU)** and **The Foundation for Scientific and Industrial Research at the Norwegian Institute of Technology (SINTEF)** as research partners.

StormGeo[84] provides customers with Wildfire Risk Assessment[85] reports on active fire's size, smoke, and air quality, and forecasts the risk of a fire developing or spreading. Finally, industry and customers, e.g., those working in the forestry and energy sectors, as well as insurance companies, farmers, media, and public are to be mentioned.

---

[78] https://ec.europa.eu/transparency/regexpert/index.cfm?do=groupDetail.groupDetail&groupID=416

[79] https://cicero.oslo.no/en/posts/projects/exhaustion

[80] https://cicero.oslo.no/en/posts/projects/acrobear-high-latitude-risk-of-wildfire-and-disease

[81] https://www.hvl.no/en/project/660212/

[82] https://fric.no/en

[83] https://risefr.com/services/research-and-assessments/fric-fire-research-and-innovation-centre

[84] https://www.stormgeo.com/

[85] https://www.stormgeo.com/solutions/data-science/wildfire-risk-assessment/

7 References

Abatzoglou, J.T., Williams, A.P., and Barbero, R. (2019). Global Emergence of Anthropogenic Climate Change in Fire Weather Indices. *Geophys. Res. Lett., 46(1)*, 326–336, doi:10.1029/2018gl080959.

Akagi, S.K., Yokelson, R.J., Wiedinmyer, C., Alvarado, M.J., Reid, J.S., Karl, T., Crounse, J.D., and Wennberg, P.O. (2011). Emission factors for open and domestic biomass burning for use in atmospheric models. *Atmos. Chem. Phys., 11,* 4039–4072, doi:10.5194/acp-11-4039-2011.

AMAP (2021). Impacts of Short-lived Climate Forcers on Arctic Climate, Air Quality, and Human Health. Summary for Policy-makers. Arctic Monitoring and Assessment Programme (AMAP), Tromsø, Norway. 20 pp., available at: https://www.amap.no/documents/doc/impacts-ofshort-lived-climate-forcers-on-arctic-climate-air-quality-andhuman-health.-summary-for-policy-makers/3512 (last access: 22 April 2022).

Andreae, M.O. and Merlet, P. (2001). Emission of trace gases and aerosols from biomass burning. *Global Biogeochem. Cy., 15,* 955–966, doi:10.1029/2000GB001382.

Andreae, M.O. (2019). Emission of trace gases and aerosols from biomass burning – an updated assessment. *Atmos. Chem. Phys., 19,* 8523–8546, doi:10.5194/acp-19-8523-2019.

Belenguer-Plomer, M.A., Tanase, M.A., Fernandez-Carrillo, A., Chuvieco, E. (2019). Burned area detection and mapping using Sentinel 1 backscatter coefficient and thermal anomalies. *Remote Sens. Environ., 233,* 111345, doi:10.1016/j.rse.2019.111345.

Boer, M.M., Resco de Dios, V., and Bradstock, R.A. (2020). Unprecedented burn area of Australian mega forest fires. *Nat. Clim. Chang., 10,* 171–172, doi:10.1038/s41558-020-0716-1.

Botnen, D.C. (2021). Country report for Norway, in San-Miguel-Ayanz et al. (eds), Forest Fires in Europe, Middle East and North Africa 2020, EUR 30862 EN, Publications Office of the European Union, Luxembourg, doi:10.2760/216466, JRC126766.

CEOS, The Joint CEOS/CGMS Working Group on Climate (WGClimate) (2018). Updated version of the Space Agency Response to GCOS Implementation Plan, Version 2.21, ESA-ECO-EOPS-WGCL-RP-17-0061, https://ceos.org/observations/documents/Space_Agency_Response_to_GCOS_IP_v2.2.1.pdf (last accessed: 17 April 2022).

Chuvieco, E., Yue, C., Heil, A., Mouillot, F., Alonso-Canas, I., Padilla, M., Pereira, J.M., Oom, D. and Tansey, K. (2016). A new global burned area product for climate assessment of fire impacts. *Global Ecol. Biogeogr., 25,* 619-629, doi:10.1111/geb.12440.

Chuvieco, E., Mouillot, F., van der Werf, G.R., San Miguel, J., Tanase, M., Koutsias, N., García, M., Yebra, M., Padilla, M., Gitas, I., Heil, A., Hawbaker, T.D., and Giglio, L. (2019). Historical background and current developments for mapping burned area from satellite Earth observation. *Remote Sens. Environ., 225,* 45-64, doi:10.1016/j.rse.2019.02.013.

Ciavarella, A., Cotterill, D., Stott, P., Kew, S., Philip, S., Van Oldenborgh, G.J., Skålevåg, A., Lorenz, P., Robin, Y., Friederike Otto, F., Hauser, M., Seneviratne, S.I., Lehner, F., and Zolina, O. (2020). Prolonged Siberian Heat of 2020. World Weather Attribution. Published online https://www.worldweatherattribution.org/wp-content/uploads/WWA-Prolonged-heat-Siberia-2020.pdf, (last accessed: 16 April 2022).

Csiszar, I., Schroeder, W., Giglio, L., Ellicott, E., Vadrevu, K.P., Justice, C.O., and Wind, B. (2014). Active fires from the Suomi NPP Visible Infrared Imaging Radiometer Suite: Product status and first evaluation results. *J. Geophys. Res. Atmos., 119,* doi:10.1002/2013JD020453.

Dell'Aglio D.A.G., Gargiulo M., Iodice A., Riccio D., Ruello G. (2019). Active fire detection in multispectral super-resolved sentinel-2 images by means of sam-based approach. In: 2019 IEEE

5th international forum on research and technology for society and industry (RTSI), 9–12 Sept 2019. 124–127, doi:10.1109/rtsi.2019.8895538.

Dozier, J.A. (1981). Method for Satellite Identification of Surface Temperature Fields of Subpixel Resolution. *Remote Sens. Environ. 11,* 221–119, https://doi.org/10.1016/0034-4257(81)90021-3.

DSB, Thema (2019). Skogbrannsesongen 2018, Erfaringer og læringspunkter. Direktoratet for samfunnssikkerhet og beredskap, https://www.dsb.no/globalassets/dokumenter/rapporter/ skogbrannsesongen_2018.pdf (last accessed: 16 April 2022).

Duncan, B.N., Ott, L.E., Abshire, J.B., Brucker, L., Carroll, M.L., Carton, J., Comiso, J.C., Dinnat, P., Forbes, E.P., Gonsamo, B.C., Gregg, A., Hall, W.W., Ialongo, D.K., Jandt, I., Kahn, R., Karpechko, R.A., Kawa, A., Kato, S.R., Kumpula, T., Kyrölä, E., Loboda, T.V., McDonald, K.C., Montesano, P.M., Nassar, R., Neigh, C.S.R., Parkinson, C.L., Poulter, B., Pulliainen, J., Rautiainen, K., Rogers, B.M., Rousseaux, C.S., Soja, A.J., Steiner, N., Tamminen, J., Taylor, P.C., Tzortziou, M.A., Virta, H., Wang, J.S., Watts, J.D., Winker, D.M., and Wu, D.L. (2020). Space-Based Observations for Understanding Changes in the Arctic-Boreal Zone. *Rev. Geophys., 58,* e2019RG000652, doi:10.1029/2019RG000652.

Duncanson, L., Armston, J., Disney, M., Avitabile, V., Barbier, N., Calders, K., Carter, S., Chave, J., Herold, M., MacBean, N., McRoberts, R., Minor, D., Paul, K., Réjou-Méchain, M., Roxburgh, S., Williams, M., Albinet, C., Baker, T., Bartholomeus, H., Bastin, J.F., Coomes, D., Crowther, T., Davies, S., de Bruin, S., De Kauwe, M., Domke, G., Dubayah, R., Falkowski, M., Fatoyinbo, L., Goetz, S., Jantz, P., Jonckheere, I., Jucker, T., Kay, H., Kellner, J., Labriere, N., Lucas, R., Mitchard, E., Morsdorf, F., Naesset, E., Park, T., Phillips, O.L., Ploton, P., Puliti, S., Quegan, S., Saatchi, S., Schaaf, C., Schepaschenko, D., Scipal, K., Stovall, A., Thiel, C., Wulder, M.A., Camacho, F., Nickeson, J., Román, M., Margolis, H. (2021). Above ground Woody Biomass Product Validation Good Practices Protocol. Version 1.0. In L. Duncanson, M. Disney, J. Armston, J. Nickeson, D. Minor, and F. Camacho (Eds.), Good Practices for Satellite Derived Land Product Validation, (p. 236): Land Product Validation Subgroup (WGCV/CEOS), doi:10.5067/doc/ceoswgcv/lpv/agb.001.

Drysdale, D. (1998). An Introduction to Fire Dynamics, 2nd Ed. John Wiley & Sons, Chichester, UK.

Eck, T.F., Holben, B.N., Reid, J.S., Sinyuk, A., Hyer, E.J., O'Neill, N.T., Shaw, G.E., Vande Castle, J.R., Chapin, F.S., Dubovik, O., Smirnov, A., Vermote, E., Schafer, J.S., Giles, D., Slutsker, I., Sorokine, M., and Newcomb, W.W. (2009). Optical properties of boreal region biomass burning aerosols in central Alaska and seasonal variation of aerosol optical depth at an Arctic coastal site. *J. Geophys. Res. - Atmos., 114,* D11201, doi:10.1029/2008JD010870.

Eckhardt, S., Breivik, K., Manø, S., and Stohl, A. (2007). Record high peaks in PCB concentrations in the Arctic atmosphere due to long-range transport of biomass burning emissions. *Atmos. Chem. Phys., 7,* 4527–4536, doi:10.5194/acp-7-4527- 2007.

Elvidge, C.D., Zhizhin, M., Hsu, F.-C., Baugh, K.E. (2013). VIIRS nightfire: Satellite pyrometry at night. *Remote Sens., 5,* 4423–4449, doi:10.3390/rs5094423.

Engelmann, R., Ansmann, A., Ohneiser, K., Griesche, H., Radenz, M., Hofer, J., Althausen, D., Dahlke, S., Maturilli, M., Veselovskii, I., Jimenez, C., Wiesen, R., Baars, H., Bühl, J., Gebauer, H., Haarig, M., Seifert, P., Wandinger, U., and Macke, A. (2021). Wildfire smoke, Arctic haze, and aerosol effects on mixed-phase and cirrus clouds over the North Pole region during MOSAiC: an introduction. *Atmos. Chem. Phys., 21,* 13397–13423, doi:10.5194/acp-21-13397-2021.

Evangeliou, N., Balkanski, Y., Hao, W. M., Petkov, A., Silverstein, R.P., Corley, R., Nordgren, B.L., Urbanski, S.P., Eckhardt, S., Stohl, A., Tunved, P., Crepinsek, S., Jefferson, A., Sharma, S., Nøjgaard, J.K., and Skov, H. (2016). Wildfires in northern Eurasia affect the budget of black carbon in the Arctic – a 12-year retrospective synopsis (2002–2013). *Atmos. Chem. Phys., 16,* 7587–7604, doi:10.5194/acp-16-7587-2016.

Evangeliou, N., Kylling, A., Eckhardt, S., Myroniuk, V., Stebel, K., Paugam, R., Zibtsev, S., and Stohl, A. (2019). Open fires in Greenland in summer 2017: transport, deposition and radiative effects of BC, OC and BrC emissions. *Atmos. Chem. Phys., 19,* 1393–1411, doi:10.5194/acp-19-1393-2019.

Franquesa, M., Vanderhoof, M.K., Stavrakoudis, D., Gitas, I.Z., Roteta, E., Padilla, M., Chuvieco, E. (2020). Development of a standard database of reference sites for validating global burned area products. *Earth Sys. Sci. Data, 12,* 3229-3246, doi:10.5194/essd-12-3229-2020.

Franquesa, M., Lizundia-Loiola, J., Stehman, S.V., Chuvieco, E. (2022). Using long temporal reference units to assess the spatial accuracy of global satellite derived burned area products. *Remote Sens. Environ. 269,* 112823, doi:10.1016/j.rse.2021.112823.

Fromm, M., Lindsey, D.T., Servranckx, R., Yue, G., Trickl, T., Sica, R., Doucet, P., and Godin-Beekmann, S. (2010). The Untold Story of Pyrocumulonimbus. *Bull. Am. Meteorol. Soc., 91,* 1193–1210, doi:10.1175/2010BAMS3004.1.

Fusco, E.J., Finn, J.T., Abatzoglou, J.T., Balch, J.K., Dadashi, S., and Bradley, B.A. (2019). Detection rates and biases of fire observations from MODIS and agency reports in the conterminous United States. *Remote Sens. Environ., 220,* 30–40, doi:10.1016/j.rse.2018.10.028.

GCOS (2016). The Global Observing System for Climate: Implementation Needs. GCOS-200, World Meteorological Organization, Geneve, Switzerland.

Glatthor, N., Höpfner, M., Semeniuk, K., Lupu, A., Palmer, P.I., McConnell, J.C., Kaminski, J.W., von Clarmann, T., Stiller, G.P., Funke, B., Kellmann, S., Linden, A., and Wiegele, A. (2013). The Australian bushfires of February 2009: MIPAS observations and GEM-AQ model results. *Atmos. Chem. Phys., 13,* 1637–1658, doi:10.5194/acp-13-1637-2013.

Gibson, C.M., Chasmer, L.E., Thompson, D.K., Quinton, W.L., Flannigan, M.D., and Olefeldt, D. (2018). Wildfire as a major driver of recent permafrost thaw in boreal peatlands. *Nat. Commun., 9,* 1–9, doi:10.1038/s41467-018-05457-1.

Giglio, L., and Kendall, J.D. (2001). Application of the Dozier retrieval to wildfire characterization: A sensitivity analysis. *Remote Sens. Environ., 77,* 34–49, doi:10.1016/S0034-4257(01)00192-4.

Giglio, L., Descloitres, J., Justice, C.O., and Kaufman, Y.J. (2003). An enhanced contextual fire detection algorithm for MODIS. *Remote Sens. Environ., 87,* 273–282, doi:10.1016/S0034-4257(03)00184-6.

Giglio, L., Csiszar, I., Justice, C.O. (2006). Global distribution and seasonality of active fires as observed with the Terra and Aqua Moderate Resolution Imaging Spectroradiometer (MODIS) sensors. *J. Geophys. Res., 111,* 1–12, doi:10.1029/2005JG000142.

Giglio, L., Csiszar, I., Restás, Á., Morisette, J.T., Schroeder, W., Morton, D., Justice, C.O. (2008). Active fire detection and characterization with the advanced spaceborne thermal emission and reflection radiometer (ASTER). *Remote Sens. Environ., 112,* 3055–3063, doi:10.1016/j.rse.2008.03.003.

Giglio, L., Loboda, T., Roy, D.P., Quayle, B., Justice, C.O. (2009). An active-fire based burned area mapping algorithm for the MODIS sensor. *Remote Sens. Environ., 113,* 408–420, doi:10.1016/j.rse.2008.10.006.

Giglio L., Schroeder W., Justice C.O. (2016). The collection 6 MODIS active fire detection algorithm and fire products. *Remote Sens. Environ., 178,* 31–41, doi:10.1016/j.rse.2016.02.054.

Giglio, L., Boschetti, L., Roy, D.P., Humber, M.L., Justice, C.O. (2018). The Collection 6 MODIS burned area mapping algorithm and product. *Remote Sens. Environ., 217,* 72–85, doi:10.1016/j.rse.2018.08.005.

Giglio, L., Schroeder, W., Hall, J.V., Justice C.O. (2022). MODIS Collection 6 Active Fire Product User's Guide Revision C, online: https://modis-fire.umd.edu/files/MODIS_C6_Fire_User_Guide_C.pdf (last accessed 22 April 2022).

Ginoux, P., and Torres, O. (2003). Empirical TOMS index for dust aerosol: Applications to model validation and source characterization. *J. Geophys. Res., 108* (D17), 4534, doi:10.1029/2003JD003470.

Gromny, E., Lewiński, S., Rybicki, M., Malinowski, R., Krupiński, M., Nowakowski, A., and Jenerowicz, M. (2019). Creation of training dataset for Sentinel-2 land cover classification, in: Photonics Applications in Astronomy, Communications, Industry, and High-Energy Physics Experiments 2019, Vol. 11176*,* p. 111763D, International Society for Optics and Photonics.

Groot Zwaaftink, C.D., Aas, W., Eckhardt, S., Evangeliou, N., Hamer, P., Johnsrud, M., Kylling, A., Platt, S.M., Stebel, K., Uggerud, H., and Yttri, K.E. (2022). What caused a record high PM_{10} episode in northern Europe in October 2020 ?. *Atmos. Chem. Phys., 22,* 3789–3810, doi:10.5194/acp-22-3789-2022.

Herman, J.R., and Celarier, E. (1997). Earth surface reflectivity climatology at 340 and 380 nm from TOMS data, *J. Geophys. Res., 102,* 28003-28011, doi:10.1029/97JD02074.

Hislop, S., Haywood, A., Jones, S., Soto-Berelov, M., Skidmore, A., and Nguyen, T.H. (2020). A satellite data driven approach to monitoring and reporting fire disturbance and recovery across boreal and temperate forests. *Int. J. Appl. Earth Obs., 87,* 102034, doi:10.1016/j.jag.2019.102034.

Hu, Y., Fernandez-Anez, N., Smith, T.E., and Rein, G. (2018). Review of emissions from smouldering peat fires and their contribution to regional haze episodes. *Int. J. Wildland Fire, 27,* 293, doi:10.1071/wf17084.

Hugelius, G., Loisel, J., Chadburn, S., Jackson, R.B., Jones, M., MacDonald, G., Marushchak, M., Olefeldt, D., Packalen, M., Siewert, M.B., and Treat, C. (2020). Large stocks of peatland carbon and nitrogen are vulnerable to permafrost thaw. *P. Natl. Acad. Sci., 117,* 20438, doi:10.1073/pnas.1916387117.

Holloway, J.E., Lewkowicz, A.G., Douglas, T.A., Li, X., Turetsky, M.R., Baltzer, J.L., and Jin, H. (2020). Impact of wildfire on permafrost landscapes: A review of recent advances and future prospects. *Permafrost Periglac., 31,* 371–382, doi:10.1002/ppp.2048.

Ichoku, C., and Ellison, L. (2014). Global top-down smoke-aerosol emissions estimation using satellite fire radiative power measurements. *Atmos. Chem. Phys., 14,* 13, 6643–6667. doi:10.5194/acp-14-6643-2014.

IPCC (2021). Summary for Policymakers. In: Climate Change 2021: The Physical Science Basis. Contribution of Working Group I to the Sixth Assessment Report of the Intergovernmental Panel on Climate Change [Masson-Delmotte, V., P. Zhai, A. Pirani, S.L. Connors, C. Péan, S. Berger, N. Caud, Y. Chen, L. Goldfarb, M.I. Gomis, M. Huang, K. Leitzell, E. Lonnoy, J.B.R. Matthews, T.K. Maycock, T. Waterfield, O. Yelekçi, R. Yu, and B. Zhou (eds.)].

Johnston, J.M., Johnston, L.M., Wooster, M.J., Brookes, A., Mc-Fayden, C., and Cantin, A.S. (2018). Satellite detection limitations of sub-canopy smouldering wildfires in the North American Boreal Forest. *Fire, 1,* 28, doi:10.3390/fire1020028.

Johnson, M.S., Strawbridge, K., Knowland, K.E., Keller, C., and Travis, M. (2021). Long-range transport of Siberian biomass burning emissions to North America during FIREX-AQ. *Atmos. Environ., 252,* 118241, doi:10.1016/j.atmosenv.2021.118241.

Justice, C.O., Giglio, L., Korontzi, S., Owens, J., Morisette, J., Roy, D., Descloitres, J., Alleaume, S., Petitcolin, F. and Kaufman, Y.J. (2002). The MODIS fire products. *Remote Sens. Environ., 83,* 244-262, doi:10.1016/S0034-4257(02)00076-7.

Justice, C.O., L. Giglio Roy, D., Boschetti, L., Csiszar, I., Davies, D., Korontzi, S., Schroeder, W., O'Neal, K., and Morisette, J. (2011). MODIS-Derived Global Fire Products. In: Ramachandran, B., Justice, C., Abrams, M. (eds) Land Remote Sensing and Global Environmental Change. Remote Sensing and Digital Image Processing, vol 11. Springer, New York, NY, doi:10.1007/978-1-4419-6749-7_29.

Justice, C.O., Giglio, L., Korontzi, S., Owens, J., Morisette, J.T., Roy, D., Descloitres, J., Alleaume, S., Petitcolin, F., and Kaufman, Y. (2020). The MODIS fire products. *Remote Sens. Environ., 83,* 1-2, 244–262, doi:10.1016/s0034-4257(02)00076-7.

Kabanov, D.M., Ritter, C., and Sakerin, S.M. (2020). Interannual and seasonal variations in the aerosol optical depth of the atmosphere in two regions of Spitsbergen (2002–2018). *Atmos. Meas. Tech., 13,* 5303–5317, doi:10.5194/amt-13-5303-2020.

Kaiser, J.W., Heil, A., Andreae, M.O., Benedetti, A., Chubarova, N., Jones, L., Morcrette, J.J., Razinger, M., Schultz, M.G., Suttie, M., and Van Der Werf, G.R. (2012). Biomass burning emissions estimated with a global fire assimilation system based on observed fire radiative power. *Biogeosciences, 9,* 527–554, doi:10.5194/bg-9-527-2012.

Kaufman, Y.J., Justice, C.O., Flynn, L.P., Kendall, J.D., Prins, E.M., Giglio, L., Ward, D.E., Menzel, W.P., and Setzer, A.W. (1998). Potential global fire monitoring from EOS-MODIS. *J. Geophys. Res., 103,* 32215–32238, doi:10.1029/98JD01644.

Keegan, K.M., Albert, M.R., McConnell, J.R., and Baker, I. (2014). Climate change and forest fires synergistically drive widespread melt events of the Greenland Ice Sheet. *P. Natl. Acad. Sci. USA, 111,* 7964, doi:10.1073/pnas.1405397111.

KCL (2019). Sentinel-3 optical products and algorithm definition, Active Fire: Fire Detection and Fire Radiative Power, version 4.3, 31 Oct 2019, S3-L2-SD-03-T04-KCL-ATBD_FIREPRODUCT, King's College London, London.

Kloss, C., Sellitto, P., von Hobe, M., Berthet, G., Smale D., Krysztofiak G., Xue C., Qiu C., Jégou F., Ouerghemmi I., Legras B. (2021). Australian Fires 2019–2020: Tropospheric and Stratospheric Pollution Throughout the Whole Fire Season. Front. *Environ. Sci., 9,* doi:10.3389/fenvs.2021.652024.

Koster, R.D., Darmenov, A., and da Silva, A. (2015). The Quick Fire Emissions Dataset (QFED): Documentation of versions 2.1, 2.2 and 2.4, NASA Technical Report Series on Global Modeling and Data Assimilation NASA TM-2015-104606, Volume 38, http://gmao.gsfc.nasa.gov/pubs/docs/Darmenov796.pdf, (last accessed: 22 April 2022).

Kumar, S.S., and Roy, D.P. (2018). Global operational land imager Landsat-8 reflectance-based active fire detection algorithm. *Int. J. Digit. Earth, 11:2,* 154-178, doi:10.1080/17538947.2017.1391341.

Kumar, S.S., Hult, J., Picotte, J., and Peterson, B. (2020). Potential Underestimation of Satellite Fire Radiative Power Retrievals over Gas Flares and Wildland Fires. *Remote Sens., 12,* 238, doi:10.3390/rs12020238.

Liu, X., Zhi, W., Xu, B., Xu, W., and Wu, W. (2021). Detecting high-temperature anomalies from Sentinel-2 MSI images. *ISPRS J.* Photogramm. *Remote Sens., 177,* 174-193, doi:10.1016/j.isprsjprs.2021.05.008.

Liu, T. (2020). Fire Inventories: Regional Evaluation, Comparison, and Metrics (FIRECAM) Tool, Earth Engine Apps [data], available at: https://globalfires.earthengine.app/view/firecam (last accessed: 22 April 2022).

Liu, T., Mickley, L.J., Marlier, M.E., De Fries, R.S., Khan, M.F., Latif, M.T., and Karambelas, A. (2020). Diagnosing spatial biases and uncertainties in global fire emissions inventories: Indonesia as regional case study. *Remote Sens. Environ., 237,* 111557, doi:10.1016/j.rse.2019.111557.

Lizundia-Loiola, J., Otón, G., Ramo, R., Chuvieco, E. (2020). A spatio-temporal active-fire clustering approach for global burned area mapping at 250 m from MODIS data. *Remote Sens. Environ., 236,* 111493, doi:10.1016/j.rse.2019.111493.

Lizundia-Loiola, J., Franquesa, M., Boettcher, M., Kirches, G., Pettinari, M.L., Chuvieco E. (2021). Implementation of the Burned Area Component of the Copernicus Climate Change Service: From MODIS to OLCI Data. *Remote Sens.,* 13 (21), 4295, doi:10.3390/rs13214295.

Lund Myhre, C., Toledano, C., Myhre, G., Stebel, K., Yttri, K.E., Aaltonen, V., Johnsrud, M., Frioud, M., Cachorro, V., de Frutos, A., Lihavainen, H., Campbell, J.R., Chaikovsky, A.P., Shiobara, M., Welton, E.J., and Tørseth, K. (2007). Regional aerosol optical properties and radiative impact of the extreme smoke event in the European Arctic in spring 2006. *Atmos. Chem. Phys., 7,* 5899–5915, doi:10.5194/acp-7-5899-2007.

Mangeon, S., Field, R., Fromm, M., McHugh, C., and Voulgarakis, A. (2015). Satellite versus ground-based estimates of burned area: A comparison between MODIS based burned area and fire agency reports over North America in 2007. *The Anthropocene Review, 3(2),* 76–92, doi:10.1177/2053019615588790.

Markowicz, K.M., Pakszys, P., Ritter, C., Zielinski, T., Udisti, R., Cappelletti, D., Mazzola, M., Shiobara, M., Xian, P., Zawadzka, O., Lisok, J., Petelski, T., Makuch, P., and Karasiński, G. (2016). Impact of North American intense fires on aerosol optical properties measured over the European Arctic in July 2015, *J. Geophys. Res. Atmos., 121,* 14,487–14,512, doi:10.1002/2016JD025310.

Markowicz, K.M., Lisok, J., and Xian, P. (2017). Simulations of the effect of intensive biomass burning in July 2015 on Arctic radiative budget. *Atmos. Environ., 171,* 248-260, doi:10.1016/j.atmosenv.2017.10.015.

Masek, J.G., Wulder, M.A., Markham, B., McCorkel, J., Crawford, C.J., Storey, J., and Jenstrom, D.T. (2020). Landsat 9: Empowering open science and applications through continuity. *Remote Sens. Environ., 248,* doi:10.1016/j.rse.2020.111968.

McCarty, J.L., Smith, T.E.L., and Turetsky, M.R. (2020). Arctic fires re-emerging. *Nature Geoscience, 13(10),* 658-660, doi:10.1038/s41561-020-00645-5.

McCarty, J.L., Aalto, J., Paunu, V.-V., Arnold, S.R., Eckhardt, S., Klimont, Z., Fain, J.J., Evangeliou, N., Venäläinen, A., Tchebakova, N.M., Parfenova, E.I., Kupiainen, K., Soja, A.J., Huang, L., and Wilson, S. (2021). Reviews and syntheses: Arctic fire regimes and emissions in the 21st century. *Biogeosciences, 18,* 5053–5083, doi:10.5194/bg-18-5053-2021.

Miller, A.N., Raudabaugh, D.B., Iturriaga, T., Matheny, P.B., Petersen, R.H., Hughes, K.W., Gube, M., Powers, R.A., James, T.Y., and O'Donnell, K. (2017). First report of the post-fire morel Morchella exuberans in eastern North America. *Mycologia, 109,* 710-714, doi:10.1080/00275514.2017.1408294.

Moroni, B., Cappelletti, D., Crocchianti, S., Becagli, S., Caiazzo, L., Traversi, R., Udisti, R., Mazzola, M., Markowicz, K., Ritter, C., and Zielinski, T. (2017). Morphochemical characteristics and mixing state of long range transported wildfire particles at Ny-Ålesund (Svalbard Islands). *Atmos. Environ., 156,* 135-145, doi:10.1016/j.atmosenv.2017.02.037.

Moroni, B., Ritter, C., Crocchianti, S., Markowicz, K., Mazzola, M., Becagli, S., Traversi, R., Krejci, R., Tunved, P., and Cappelletti, D. (2020). Individual Particle Characteristics, Optical Properties and Evolution of an Extreme Long-Range Transported Biomass Burning Event in the European Arctic (Ny-Ålesund, Svalbard Islands). *J. Geophy. Res. - Atmos., 125*, 5, doi:10.1029/2019JD031535.

Murphy, S.W., de Souza Filho, C.R., Wright, R., Sabatino, G., Pabon, R.C. (2016). HOTMAP: Global hot target detection at moderate spatial resolution. *Remote Sens. Environ., 177,* 78-88, doi:10.1016/j.rse.2016.02.027.

Myhre, C.L., Svendby, T.M., Hermansen, O., Lunder, C.R., Platt, S.M., Fiebig, M., Fjæraa, A.M., Hansen, G.H., Schmidbauer, N., and Krognes, T. (2020). Monitoring of greenhouse gases and aerosols at Svalbard and Birkenes in 2019. Annual report, NILU rapport, 16/2020, NILU, Kjeller, Norway. https://hdl.handle.net/11250/2689192.

Oliva P., and Schroeder W. (2015). Assessment of VIIRS 375 m active fire detection product for direct burned area mapping. *Remote Sens. Environ., 160,* 144–155, doi:10.1016/j.rse.2015.01.010.

Ohneiser, K., Ansmann, A., Chudnovsky, A., Engelmann, R., Ritter, C., Veselovskii, I., Baars, H., Gebauer, H., Griesche, H., Radenz, M., Hofer, J., Althausen, D., Dahlke, S., and Maturilli, M. (2021). The unexpected smoke layer in the High Arctic winter stratosphere during MOSAiC 2019 – 2020. *Atmos. Chem. Phys., 21,* 15783–15808, doi:10.5194/acp-21-15783-2021.

Osterkamp, T.E. (2005). The recent warming of permafrost in Alaska. *Global and Planetary Change, 49 (3-4),* 187-202, doi:10.1016/j.gloplacha.2005.09.001.

Otón, G., Lizundia-Loiola, J., Pettinari, M.L., Chuvieco, E. (2021a). Development of a consistent global long-term burned area product (1982–2018) based on AVHRR-LTDR data. *Int. J. App. Earth Obs. Geoinf., 103,* 102473, doi:10.1016/j.jag.2021.102473.

Otón, G., Pereira, J.M.C., Silva, J.M.N., Chuvieco, E. (2021b). Analysis of trends in the FireCCI global long term burned area product (1982-2018). *Fire 4*(4), 74, doi:10.3390/fire4040074.

Pan, X., Ichoku, C., Chin, M., Bian, H., Darmenov, A., Colarco, P., Ellison, L., Kucsera, T., da Silva, A., Wang, J., Oda, T., and Cui, G. (2020). Six global biomass burning emission datasets: intercomparison and application in one global aerosol model. *Atmos. Chem. Phys., 20,* 969–994, doi:10.5194/acp-20-969-2020.

Peterson, D.; Wang, J., Ichoku, C., Hyer, E., Ambrosia, V. (2013). A sub-pixel-based calculation of fire radiative power from MODIS observations: 1: Algorithm development and initial assessment. *Remote Sens. Environ., 129,* 262–279, doi:10.1016/j.rse.2012.10.036.

Pettinari, M.L., and Chuvieco, E. (2020). Fire Danger Observed from Space. *Surv. Geophys., 41,* 1437–1459, doi:10.1007/s10712-020-09610-8.

Pickell, P.D., Coops, N.C., Ferster, C.J., Bater, C.W., Blouin, K.D., Flannigan, M.D., and Zhang, J. (2017). An early warning system to forecast the close of the spring burning window from satellite-observed greenness. *Sci. Rep., 7,* 14190, doi:10.1038/s41598-017-14730-0.

Raynolds, M.K., Walker, D.A., Balser, A., Bay, C., Campbell, M., Cherosov, M.M., Daniëls, F.J.A., Eidesen, P.B., Ermokhina, K.A., Frost, G.V., Jedrzejek, B., Jorgenson, M.T., Kennedy, B.E., Kholod, S.S., Lavrinenko, I.A., Lavrinenko, O.V., Magnússon, B., Matveyeva, N.V., Metúsalemsson, S., Nilsen, L., Olthof, I., Pospelov, I.N., Pospelova, E.B., Pouliot, D., Razzhivin, V., Schaepman-Strub, G., Šibík, J., Telyatnikov, M.Y., and Troeva, E. (2019). A raster version of the Circumpolar Arctic Vegetation Map (CAVM). *Remote Sens. Environ., 232,* 111297, doi:10.1016/j.rse.2019.111297.

Randerson, J.T., Chen, Y., van der Werf, G.R., Rogers, B.M., and Morton, D.C. (2012). Global burned area and biomass burning emissions from small fires. *J. Geophys. Res., 117,* G04012, doi:10.1029/2012JG002128.

Ranjbar, K., O'Neill, N.T., Lutsch, E., McCullough, E.M., AboEl-Fetouh, Y., Xian, P., Strong, K., Fioletov, V.E., Lesins, G., and Abboud,I. (2019). Extreme smoke event over the high Arctic. *Atmos. Environ., 218,* 117002*,* doi:10.1016/j.atmosenv.2019.117002.

Rein, G., Cleaver, N., Ashton, C., Pironi, P., and Torero, J.L. (2008). The severity of smouldering peat fires and damage to the forest soil. *Catena, 74,* 304–309, doi:10.1016/j.catena.2008.05.008.

Rein, G. (2016). Smoldering combustion, in: SFPE Handbook of Fire Protection Engineering, edited by: Hurley, M.J., Gottuk, D., Hall, J.R., Harada, K., Kuligowski, E., Puchovsky, M., Torero, J.,Watts, J.M., and Wieczoreks, C., Springer New York, New York, 581–603, doi:10.1007/978-1-4939-2565-0_19.

Ritter, C., Angeles Burgos, M., Böckmann, C., Mateos, D., Lisok, J., Markowicz, K.M., Moroni, B., Cappelletti, D., Udisti, R., Maturilli, M., and Neuber, R. (2018). Microphysical properties and radiative impact of an intense biomass burning aerosol event measured over Ny-Ålesund, Spitsbergen in July 2015. *Tellus B: Chem. Phys. Meteorol., 70:1*, 1-23, doi: 10.1080/16000889.2018.1539618.

Roberts, G.J., and Wooster, M.J. (2008). Fire detection and fire characterization over Africa using Meteosat SEVIRI, IEEE Trans. *Geosci. Remote Sens., 46,* 1200–1218, doi:10.1109/TGRS.2008.915751.

Rogers, B.M., Balch, J.K., Goetz, S.J., Lehmann, C.E., and Turetsky, M. (2020). Focus on changing fire regimes: interactions with climate, ecosystems, and society. *Environ. Res. Lett., 15,* 030201, doi:10.1088/1748-9326/ab6d3a.

Roteta, E., Bastarrika, A., Padilla, M., Storm, T., and Chuvieco, E. (2019). Development of a Sentinel-2 burned area algorithm: Generation of a small fire database for sub-Saharan Africa. *Remote Sens. Environ., 222,* 1-17, doi:10.1016/j.rse.2018.12.011.

Roy, D.P., Huang, H., Boschetti, L., Giglio, L., Yan, L., Zhang, H.H., Li, Z. (2019). Landsat-8 and Sentinel-2 burned area mapping - A combined sensor multi-temporal change detection approach. *Remote Sens. Environ., 231,* doi:10.1016/j.rse.2019.111254.

Sakerin, S.M., Kabanov, D.M., Makarov, V.I., Pol'kin, V.V., Popova, S.A., Chankina, O.V., Pochufarov, A.O., Radionov, V.F., Rize, D.D. (2020). Spatial Distribution of Atmospheric Aerosol Physicochemical Characteristics in the Russian Sector of the Arctic Ocean. *Atmosphere, 11*, 1170, doi:10.3390/atmos11111170.

San-Miguel-Ayanz, J., Durrant, T., Boca, R., Maianti, P., Liberta, G., Artes-Vivancos, T., Oom, D., Branco, A., de Rigo, D., Ferrari, D., Pfeiffer, H., Grecchi, R., Nuijten, D., Onida, M., Ldffler, P. (2021). Forest Fires in Europe, Middle East and North Africa 2020 EUR 30862 EN, Publications Office of the European Union, Luxembourg, doi:10.2760/216466, JRC12676.

San-Miguel-Ayanz, J., Durrant, T., Boca, R., Maianti, P., Liberta`, G., Artes Vivancos, T., Jacome Felix Oom, D., Branco, A., De Rigo, D., Ferrari, D., Pfeiffer, H., Grecchi, R., and Nuijten, D. (2022). Advance report on wildfires in Europe, Middle East and North Africa 2021, EUR 31028 EN, Publications Office of the European Union, Luxembourg, doi:10.2760/039729, JRC128678.

Schneider, P., Roberts, D. A., and Kyriakidis, P.C. (2008). A VARI-based relative greenness from MODIS data for computing the Fire Potential Index. *Remote Sens. Environ., 112(3),* 1151-1167, doi:10.1016/j.rse.2007.07.010.

Scholten, R.C., Jandt, R., Miller, E.A., Rogers, B.M., and Veraverbeke, S. (2021). Overwintering fires in boreal forests. *Nature, 593,* 399–404.

Schroeder W., Oliva P., Giglio L., Csiszar I.A. (2014). The New VIIRS 375 m active fire detection data product: algorithm description and initial assessment. *Remote. Sens. Environ., 143,* 85–96. doi:10.1016/j.rse.2013.12.008.

Schroeder W., Oliva P., Giglio L., Quayle B., Lorenz E., Morelli F. (2016). Active fire detection using Landsat-8/OLI data. *Remote Sens. Environ., 185,* 210–220, doi:10.1016/j.rse.2015.08.032.

Sizov, O., Ezhova, E., Tsymbarovich, P., Soromotin, A., Prihod'ko, N., Petäjä, T., Zilitinkevich, S., Kulmala, M., Bäck, J., and Köster, K. (2021). Fire and vegetation dynamics in northwest Siberia during the last 60 years based on high-resolution remote sensing, *Biogeosciences, 18,* 207–228, doi:10.5194/bg-18-207-2021.

Sodemann, H., Pommier, M., Arnold, S.R., Monks, S.A., Stebel, K., Burkhart, J.F., Hair, J.W., Diskin, G.S., Clerbaux, C., Coheur, P.-F., Hurtmans, D., Schlager, H., Blechschmidt, A.-M., Kristjánsson, J.E., and Stohl, A. (2011). Episodes of cross-polar transport in the Arctic troposphere during July 2008 as seen from models, satellite, and aircraft observations. *Atmos. Chem. Phys., 11*, 3631–3651, doi:10.5194/acp-11-3631-2011.

Sofan, P., Bruce, D., Schroeder, W., Jones, E., and Marsden, J. (2020). Assessment of VIIRS 375 m active fire using tropical peatland combustion algorithm applied to Landsat-8 over Indonesia's peatlands. *Int. J. Digit. Earth, 1–22*, doi:10.1080/17538947.2020.1791268.

Song, Z., Kuenzer, C., Zhu, H., Zhang, Z., Jia, J., Sun, Y., and Zhang, J. (2015). Analysis of coal fire dynamics in the Wuda syncline impacted by fire-fighting activities based on in-situ observations and Landsat-8 remote sensing data. *Int. J. Coal Geol., 141,* 91–102, doi:10.1016/j.coal.2015.03.008.

Soszyńska, A.K. (2021). Parametrisation of Gas Flares Using FireBIRD Infrared Satellite Imagery, Dissertation, Humboldt-Universität zu Berlin, Germany, 03.09.2021, http://dx.doi.org/10.18452/23299, (last assessed: 27 April 2022).

Stock, M., Ritter, C., Herber, A., von Hoyningen-Huene, W., Baibakov, K., Gräser, J., Orgis, T., Treffeisen, R., Zinoviev, N., Makshtas, A., and Dethloff, K. (2012). Springtime Arctic aerosol: Smoke versus haze, a case study for March 2008. *Atmos. Environ., 52,* 48-55, doi:10.1016/j.atmosenv.2011.06.051.

Stohl, A., Andrews, E., Burkhart, J.F., Forster, C., Herber, A., Hoch, S.W., Kowal, D., Lunder, C., Mefford, T., Ogren, J.A., Sharma, S., Spichtinger, N., Stebel, K., Stone, R., Strom, J., Tørseth, K., Wehrli, C., and Yttri, K.E. (2006). Pan-Arctic enhancements of light absorbing aerosol concentrations due to North American boreal forest fires during summer 2004. *J. Geophys. Res., 111,* D22214, doi:10.1029/2006JD007216.

Stohl, A., Berg, T., Burkhart, J.F., Fjæraa, A.M., Forster, C., Herber, A., Hov, Ø., Lunder, C., McMillan, W.W., Oltmans, S., Shiobara, M., Simpson, D., Solberg, S., Stebel, K., Ström, J., Tørseth, K., Treffeisen, R., Virkkunen, K., and Yttri, K.E. (2007). Arctic smoke – record high air pollution levels in the European Arctic due to agricultural fires in Eastern Europe in spring 2006. *Atmos. Chem. Phys., 7,* 511–534, doi:10.5194/acp-7- 511-2007.

Stone, R.S., Anderson, G.P., Shettle, E.P., Andrews, E., Loukachine, K., Dutton, E.G., Schaaf, C., and Roman III, M.O. (2008). Radiative impact of boreal smoke in the Arctic: Observed and modelled. *J. Geophys. Res., 113,* D14S16, doi:10.1029/2007JD009657.

Sullivan, A.L., Ellis, P.F., Knight, I., K. (2003). A review of radiant heat flux models used in bushfire applications. *Int. J. Wildland Fire, 12,* 101–110, doi:10.1071/WF02052.

Swanson, D.K., Sousanes, P.J., and Hill, K. (2021). Increased mean annual temperatures in 2014–2019 indicate permafrost thaw in Alaskan national parks. *Arctic, Antarctic, and Alpine Research, 53(1),* 1-19, doi:10.1080/15230430.2020.1859435.

Torres, O., Bhartia, P.K., Herman, J.R., Ahmad, Z., and Gleason, J. (1998). Derivation of aerosol properties from satellite measurements of backscattered ultraviolet radiation: Theoretical basis. *J. Geophys. Res., 103(D14),* 17,099–17,110. doi:10.1029/98JD00900.

Torres, O., Bhartia, P.K., Taha, G., Jethva, H., Das, S., Colarco, P., Krotkov, N., Omar, A., Ahn, C. (2020). Stratospheric injection of massive smoke plume from Canadian boreal fires in 2017 as seen by DSCOVR-EPIC, CALIOP, and OMPS-LP observations. *J. Geophys. Res. – Atmos., 125,* doi:10.1029/2020JD032579.

Treffeisen, R., Tunved, P., Ström, J., Herber, A., Bareiss, J., Helbig, A., Stone, R.S., Hoyningen-Huene, W., Krejci, R., Stohl, A., and Neuber, R. (2007). Arctic smoke – aerosol characteristics during a

record smoke event in the European Arctic and its radiative impact. *Atmos. Chem. Phys., 7,* 3035–3053, doi:10.5194/acp-7-3035-2007.

United Nations Environment Programme (2022). Spreading like Wildfire – The Rising Threat of Extraordinary Landscape Fires. A UNEP Rapid Response Assessment. Nairobi. https://www.unep.org/resources/report/spreading-wildfire-rising-threat-extraordinary-landscape-fires, (last assessed 23/03/2022).

van der Werf, G.R., Randerson, J.T., Giglio, L., Collatz, G.J., Kasibhatla, P.S., and Arellano Jr., A.F. (2006). Interannual variability in global biomass burning emissions from 1997 to 2004. *Atmos. Chem. Phys., 6,* 3423–3441, doi:10.5194/acp-6-3423-2006.

van der Werf, G.R., Randerson, J.T., Giglio, L., van Leeuwen, T.T., Chen, Y., Rogers, B.M., Mu, M., van Marle, M.J.E., Morton, D.C., Collatz, G.J., Yokelson, R.J., and Kasibhatla, P.S. (2017). Global fire emissions estimates during 1997–2016. *Earth Syst. Sci. Data, 9,* 697–720, doi:10.5194/essd-9-697-2017.

Veraverbeke, S., Rogers, B.M., Goulden, M.L., Jandt, R.R., Miller, C.E., Wiggins, E.B., and Randerson, J.T. (2017). Lightning as a major driver of recent large fire years in North American boreal forests. *Nat. Clim. Change, 7,* 529, doi:10.1038/nclimate3329.

Vodacek, A., Kremens, R.L., Fordham, A.J., Vangorden, S.C., Luisi, D., Schott, J.R., and Latham, D.J. (2002). Remote optical detection of biomass burning using a potassium emission signature. *Int. J. Remote Sens., 23,* 13, 2721-2726, doi:10.1080/01431160110109633.

Wiedinmyer, C., Akagi, S.K., Yokelson, R.J., Emmons, L.K., Al-Saadi, J.A., Orlando, J.J., and Soja, A.J. (2011). The Fire INventory from NCAR (FINN): a high resolution global model to estimate the emissions from open burning. *Geosci. Model Dev., 4,* 625–641, doi:10.5194/gmd-4-625-2011.

Wiedinmyer, C., Kimura, Y., McDonald-Buller, E. C., Emmons, L. K., Buchholz, R. R., Tang, W., Seto, K., Joseph, M. B., Barsanti, K. C., Carlton, A. G., and Yokelson, R. (2023). The Fire Inventory from NCAR version 2.5: an updated global fire emissions model for climate and chemistry applications. *Geosci. Model Dev.*, 16, 3873–3891, doi:10.5194/gmd-16-3873-2023.

Witze, A. (2020). The Arctic is burning like never before: and that's bad news for climate change. *Nature, 585* (7825), 336-337, doi:10.1038/d41586-020-02568-y.

Wooster, M.J., Zhukov, B., Oertel, D. (2003). Fire radiative energy for quantitative study of biomass burning: Derivation from the BIRD experimental satellite and comparison to MODIS fire products. *Remote Sens. Environ., 86,* 83–107, doi:10.1016/S0034-4257(03)00070-1.

Wooster, M.J., Roberts, G., Perry, G.L.W., Kaufman, Y.J. (2005). Retrieval of biomass combustion rates and totals from fire radiative power observations: FRP derivation and calibration relationships between biomass consumption and fire radiative energy release. *J. Geophys. Res. Atmos., 110,* doi:10.1029/2005JD006318.

Wooster, M.J., Xu, W., and Nightingale, T. (2012). Sentinel-3 SLSTR active fire detection and FRP product: Pre-launch algorithm development and performance evaluation using MODIS and ASTER datasets. *Remote Sens. Environ., 120,* 236-254, doi:10.1016/j.rse.2011.09.033.

Xu, W., Wooster, M., He, J., and Zhang, T. (2020). First Study of Sentinel-3 SLSTR Active Fire Detection and FRP Retrieval: Night-time Algorithm Enhancements and Global Intercomparison to MODIS and VIIRS AF Products. *Remote Sens. Environ., 248,* 111947, doi:10.1016/j.rse.2020.111947.

Xu, W., Scholten, R.C., Hessilt, T.D., Liu, Y., and Veraverbeke, S. (2022). Overwintering fires rising in eastern Siberia. *Environ. Res. Lett., 17* (4), 1-10, 045005, doi:10.1088/1748-9326/ac59aa.

York, A., Bhatt, U.S., Gargulinski, E., Garbinski, Z., Jain, P., Soja, A., Thoman, R.L., and Ziel, R (2020). Wildland Fire in High Northern Latitudes, in: Arctic Report Card 2020, doi:10.25923/2gef-3964.

Zielinski T., Bolzacchini E., Cataldi M., Ferrero L., Graßl S., Hansen G., Mateos D., Mazzola M., Neuber R., Pakszys P., Posyniak M., Ritter C., Severi M., Sobolewski P., Traversi R., Velasco-Merino C. (2020). Study of Chemical and Optical Properties of Biomass Burning Aerosols during Long-Range Transport Events toward the Arctic in Summer 2017. *Atmosphere*, 11(1), 84, doi:10.3390/atmos11010084.

Zhang, X., Friedl, M., and Henebry, G. (2020). *VIIRS/NPP Land Cover Dynamics Yearly L3 Global 500m SIN Grid V001*. 2020, distributed by NASA EOSDIS Land Processes DAAC, doi:10.5067/VIIRS/VNP22Q2.001.

Zhu, C., Kobayashi, H., Kanaya, Y., and Saito, M. (2017). Size-dependent validation of MODIS MCD64A1 burned area over six vegetation types in boreal Eurasia: Large underestimation in croplands. *Sci. Rep., 7,* 4181, doi:10.1038/s41598-017-03739-0.

NILU – Norwegian Institute for Air Research

NILU – Norwegian Institute for Air Research is an independent, non-profit institution established in 1969. Through its research NILU increases the understanding of climate change, of the composition of the atmosphere, of air quality and of hazardous substances. Based on its research, NILU markets integrated services and products within analysing, monitoring and consulting. NILU is concerned with increasing public awareness about climate change and environmental pollution.

NILU's values: *Integrity - Competence - Benefit to society*
NILU's vision: *Research for a clean atmosphere*

NILU – Norwegian Institute for Air Research
P.O. Box 100, NO-2027 KJELLER, Norway

E-mail: nilu@nilu.no
http://www.nilu.no

Norsk institutt for luftforskning
Norwegian Institute for Air Research